EFFECTS OF HIGH SPEED MACHINING ON SURFACE TOPOGRAPHY OF TITANIUM ALLOY (TI6AL4V)

By

ADITYA MODGIL

A THESIS PRESENTED TO THE GRADUATE SCHOOL
OF THE UNIVERSITY OF FLORIDA IN PARTIAL FULFILLMENT
OF THE REQUIREMENTS FOR THE DEGREE OF
MASTER OF SCIENCE

UNIVERSITY OF FLORIDA

2003

ACKNOWLEDGMENTS

I wish to express my appreciation to Dr. John Schueller for his support and guidance in completion of this project. Thanks are due to Dr. John Ziegert for his valuable ideas and also for serving on my supervisory committee. I would like to thank Dr. Tony Schmitz for his valuable input and for serving on my supervisory committee.

The assistance of Dr. Michael Kauffman and his student Jerry Bourne is highly appreciated in this project. I would also like to thank all the members of the Machine Tool Research Center for their help, friendship and criticism. Specifically I would like to thank Michael Tummond and Scott Duncan for their assistance in this project.

Finally I would like to thank my parents for their moral support.

TABLE OF CONTENTS

page

LIST OF TABLES

LIST OF FIGURES

Abstract of Thesis Presented to the Graduate School
Of the University of Florida in Partial Fulfillment of the
Requirements for the Degree of Masters of Science

EFFECTS OF HIGH SPEED MACHINING ON SURFACE TOPOGRAPHY OF TITANIUM ALLOY (Ti6Al4V)

By

Aditya Modgil

December 2003

Chair: John K. Schueller
Major Department: Mechanical and Aerospace Engineering

High speed machining (HSM) has been demonstrated to greatly improve the productivity of milling in manufacturing. Although widely used for manufacturing aluminum alloys in aerospace components, milling has received less use on titanium alloys. There exists a concern that high-speed machining of such alloys may leave surfaces detrimental to fatigue life.

This work investigated the geometrical properties of surfaces face milled on Ti6Al4V alloy using conventional and high speed machining processes. Workpieces were machined using high speed and conventional speed machining processes. Machined specimens were then prepared for microstructural analysis using cutting, grinding and polishing processes. Microstructural analysis was done on the specimens using an optical microscope to find the possible effects of high speed machining and conventional speed machining processes on the

grain structure. Rockwell C hardness testing was then done on the specimens to see the effect of different machining processes on the hardness of Ti6Al4V specimens.

The results presented in this work have shown that high speed machining and conventional speed machining processes produce small semi spherical defects on the machined surfaces of Ti6Al4V workpieces. The number of defects is more in the high speed machining case as compared to conventional machining case. These defects can affect the fatigue life of the components in service as these may act as areas of stress concentration and favorable sites for earlier initiation of fatigue cracks as cracks can propagate from the top of the surface to down below the sub-surface. But these defects are only a few microns in depth. A finish machining pass at a low axial depth of cut and at a low speed was made over the high speed machined area as a solution to this problem. The results have also shown that the grain size and orientation are not affected by the high speed machining and conventional machining processes if the flood coolant is used, as the temperature produced during these processes is not enough to cause the transformation of the phases.

An analysis of variance performed on the Rockwell C hardness test data strongly indicates that the hardness is affected by the HSM and conventional machining processes. But the differences in the mean values of the hardness of high speed machined and conventional speed machined specimens are small. Results have been tabulated and recommendations have been made.

CHAPTER 1
INTRODUCTION

The aerospace industry is the single largest market for titanium products primarily due to the exceptional strength-to- weight ratio, elevated temperature performance and corrosion resistance. Titanium applications are most significant in jet engine and airframe components that are subject to temperatures up to 1100° F and for other critical structural parts [1]. Usage is widespread in most commercial and military aircrafts. Generally, titanium alloys fall into four major groups, classified by their alloying elements and microstructures. They are: pure titanium (unalloyed), alpha phase, alpha beta and beta [2].The most commonly used alloys are the alpha-beta group. A member of this group, Ti6A14V, comprises more than 50 percent of all titanium alloys used today [1].

The techniques of High Speed Machining (HSM), while still in an initial stage of wide acceptance, have already been proven in leading aircraft manufacturing plants [3]. HSM has been applied successfully to materials like magnesium and aluminum. It has been proved that there are considerable savings in the machining time by comparing the conventional machining times and the high speed machining times for the magnesium test castings in one of the projects at the University of Florida's Machine Tool Research Center (MTRC) [4]. Another success of HSM can be seen in the project involving the application of the HSM techniques to machine the aluminum top cover of a helicopter gearcase. [5]. In this case too, it was shown that HSM could be implemented successfully with great reduction in machining time. The implementation of the High Speed Machining technology depends on a number of factors including the machine and tool

dynamics, work material, the power, torque and feed capabilities of the machine tool. The potential success of implementing the HSM is based on the high metal removal rate and short production times. One of the projects at MTRC involved applying high speed machining techniques to the machining processes of a helicopter rotor yoke manufactured from a solid blank of titanium alloy Ti6Al4V. Several tests were conducted using the high speed milling process with the optimized parameters in order to reduce the machining time and the machining time was shown to be reduced to 50%. The machining parameters that were used for doing the cutting tests are available in [6]. Similar machining tests were conducted at BHT (Bell Helicopter Textron) on coupons using the high speed machining parameters that were developed at UF and the coupons were also tested using conventional machining parameters developed at BHT. The process developed to machine the coupons using high speed machining parameters was termed as the advanced speed process and the process used to machine the coupons using conventional speed machining parameters was termed as conventional process. Tests showed that HSM process may result in lower fatigue strength of the coupons as compared to the conventional process.

1.1 Characteristics of Ti6Al4V Influencing Machinability

Although HSM can increase the productivity there are certain characteristics of titanium that poses limitations on its machinability. Some of these are given as follows:

1. Titanium alloy (Ti6Al4V) has low thermal conductivity, so heat does not dissipate easily from the tool-chip interface, the tool gets heated quickly due to the resulting high temperatures, and this leads to lower tool lives.

2. Titanium has a strong alloying tendency or chemical reactivity with materials in the cutting tools at tool operating temperatures. This causes welding and smearing along with rapid destruction of the cutting tool.

3. Titanium has a relatively low modulus of elasticity, thereby having more "springiness" than steel. Work has a tendency to move away from the cutting tool unless heavy cuts are maintained or proper backup is employed. Slender parts tend to deflect under tool pressures, causing chatter, tool rubbing and tolerance problems. Rigidity of the entire system is consequently very important, as is the use of sharp, properly shaped cutting tools.

The goal of this research is to determine the possible effects of high speed milling process on the Ti6Al4V surfaces by conducting the microstrutural analysis of the workpieces machined with high speed and conventional speed parameters. This includes metallographic study of the specimens under an optical microscope to analyze their size, shape and location of the defects, which might form as a result of high speed machining and conventional machining processes. These defects on the surface may lead to major changes in the mechanical properties of the material such as reduction in fatigue life. The defects are stress concentration areas and serve to act as fatigue crack initiation sites. Also, this research is intended to look for any change in the size and orientation of the grains caused by different machining processes. The results from this research will assist in the further investigation of certain phenomena like loss of fatigue life of the high speed machined Ti6Al4V specimens which may lead to the improvements in manufacturing of aerospace titanium alloys.

1.2 Brief Summary of the Research

The workpieces (made of Ti6Al4V), were machined using the machining parameters developed at Machine Tool Research Center (MTRC) from the cutting parameters used at Bell Helicopter Textron and at UF by keeping the same surface speed. Then using wire EDM, 2 specimens were taken out from each of the 3 different areas machined using 3 different set of machining parameters. Figures 1-1 shows different areas on the workpieces from where the specimens were taken out using wire EDM.

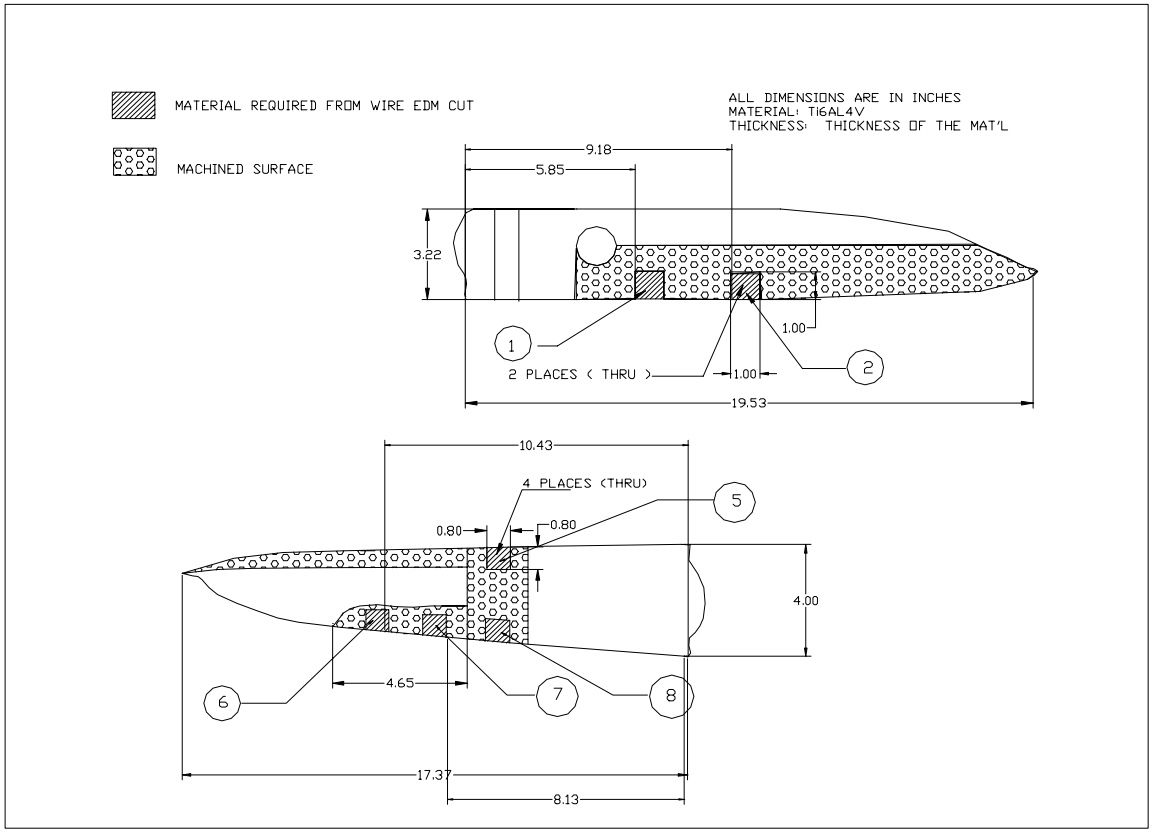

Figure 1-1 Workpieces machined using different sets of machining parameters

All the specimens from different machining areas were then subjected to Rockwell C hardness testing using a diamond indenter. Specimens were then ground and polished to reveal the microstructure. Grinding was done in different stages using granite papers of grit size 240 micron, 320 micron, 400 micron and 600 micron. Polishing was then carried

out on billiard cloth using slurry of suspension sizes of 15 micron, 5 micron, 1 micron and 0.3 micron. The specimens were then etched using Kroll's reagent to reveal the grain boundaries. Grain boundaries have high-energy spots and etching releases the electrons, which are loosely held inside the atoms to reveal the microstructure. The microstructure analysis of the specimens was then conducted under optical microscope and the pictures were taken on the machined surfaces and on the right angle to the machined surfaces of the specimens to record the size, shape and location of the defects. Also the pictures were taken to check for the changes in the size and orientation of the grains under different magnifications. Rockwell C hardness testing of the specimens was then carried out to see for the effects of HSM on the hardness of specimens. The workpiece was machined again using advance speed machining parameters and then a finish machining pass was made to remove the surface defects.

CHAPTER 2
REVIEW OF LITERATURE

The quality of a machined surface is becoming more and more important to satisfy the increasing demands of sophisticated component performance, longevity, and reliability [7]. Structures for military and commercial aerospace, automotive, and other capital goods industries are being subjected to more severe conditions of stress, temperature, and hostile environments. In response to the above needs, there has been a continued increase in the development and use of heat resistant, corrosion resistant and high strength alloys in the wide variety of structural applications. Ti6Al4V is one of the alloys of titanium that is best suited for these types of applications [7].

2.1 Titanium alloy (Ti6Al4V)

This alloy is extensively used in manufacturing of the aerospace components because of the combination of high strength-to-weight ratio, excellent fatigue properties, fracture toughness and corrosion resistance [8]. Some of its physical and mechanical properties are given in Tables 2-2 and 2-3.

Ti6Al4V is an alpha-beta alloy, the alpha phase proportion usually varies from 60 to 90%. The alpha phase in pure titanium is characterized by a hexagonal close-packed crystalline structure that remains stable from room temperature to approximately 1,620°F The beta phase in pure titanium has a body-centered cubic structure, and is stable from approximately 1,620°F to the melting point of about 3,040°F [9]. Adding alloying elements to titanium provides a wide range of physical and mechanical properties. Certain alloying additions, notably aluminum, tend to stabilize the alpha phase; that is,

they raise the temperature at which the alloy will be transformed completely to the beta phase. This temperature is known as the beta-transus temperature. Alloying additions such as chromium, copper, iron, manganese, molybdenum, and vanadium stabilize the beta phase by lowering the temperature of transformation from alpha to beta [9]. The typical microstructure is equiaxed (the same dimension in all directions), or elongated alpha grains in a transformed beta matrix [1]. Figure 2-1 shows the alpha and the transformed beta phases.

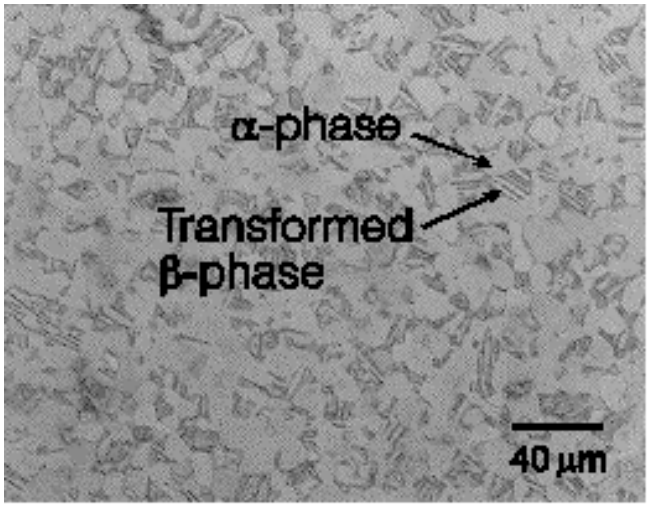

Figure 2-1 Microstructure of the primary [alpha] and transformed [beta] phases in Ti6Al4V [10]

The composition of Ti6Al4V is given in Table 2-1

Table 2-1 Composition of Ti6Al4V [2]

C	**<0.08%**
Fe	**<0.25%**
N_2	**<0.05%**
O_2	**<0.2%**
Al	**5.5-6.76%**
V	**3.5-4.5%**
Ti	**Balance**

Table 2-2 Typical physical properties for Ti6Al4V[2]

Density g/cm^3 (lb/ cu in)	4.42 (0.159)
Melting Range °C±15°C (°F)	1649 (3000)
Specific Heat J/kg.°C (BTU/lb/°F)	560 (0.134)
Volume Electrical Resistivity ohm.cm (ohm.in)	170 (67)
Thermal Conductivity W/m.K (BTU/ft.h.°F)	7.2 (67)

Ti6Al4V is the most commonly used alloy – over 70% of all alloy grades melted are a sub-grade of Ti6Al4V, its uses span many aerospace airframe and engine component uses and also major non-aerospace applications in the marine, offshore and power generation industries in particular. The addition of 0.05% palladium, (grade 24), 0.1% ruthenium (grade 29) and 0.05% palladium and 0.5% nickel (grade 25) significantly increase corrosion resistance in reducing acid, chloride and sour environments, raising the threshold temperature for attack to well over 200°C (392°F) [2].

Table 2-3 Typical mechanical properties of Ti6Al4V [2]

Hardness, Brinell	334	Estimated from Rockwell C.
Hardness, Knoop	363	Estimated from Rockwell C.
Hardness, Rockwell C	36	
Hardness, Vickers	349	Estimated from Rockwell C.
Tensile Strength, Ultimate	950 MPa	
Tensile Strength, Yield	880 MPa	
Modulus of Elasticity	113.8 GPa	
Poisson's Ratio	0.342	
Fatigue Strength	240 MPa	at 1E+7 cycles. K_t (stress concentration factor) = 3.3
Fracture Toughness	75 MPa-m½	

2.2 Importance of Surface Integrity

Dynamic loading is a principal factor in the design of many aircraft structures and accordingly design capabilities are frequently limited by the fatigue characteristic of the materials. Service histories and failure analyses of dynamic components show that fatigue failures almost always nucleate on or near the surface of a component [12]. So, much attention should be paid to surface characteristics of components. Modern production methods have been developed to more efficiently process the higher strength and high temperature alloys which have evolved in recent years. The newer high performance materials have generally become inherently "more difficult" to machine. At the same time, advanced designs have necessitated the requirement of holding closer dimensional control of larger surfaces as well as in areas of more intricate and complex geometry [12]. Since materials like Ti6Al4V require improved capabilities because of the difficulty in machining and finishing such higher strength materials, the need for paying careful attention to the surfaces of finished components is brought critically into focus.

Surface integrity is defined as the inherent or enhanced condition of a surface produced in a machining or other surface generating operation [12]. The nature of the surface layer has a strong influence on the mechanical properties of the part. When machining any component, it is first necessary to satisfy the surface integrity requirements. Surface integrity produced by a metal removal operation includes the nature of both surface topography as well as surface metallurgy. Surface integrity is concerned primarily with the host of effects a machining process produces below the visible surface. Some of these alterations are discussed as follows:

2.2.1 Types of Surface Alterations

The types of surface alterations associated with the machining processes include the following [12]:

1. Formation of notches and defects on the top surface
2. Plastic deformation of the surface layer
3. Change in hardness of the surface layer
4. Microcracking and macrocracking.
5. Residual stress distribution in the surface layer.

2.3 Previous work on the study of microstructure of Ti6Al4V

The specimens prepared for fatigue testing were acquired from Bell Helicopter Textron by the MTRC and were sectioned to look at the microstructure near the surface. The pictures of the microstructure of the specimens given in Figures 2-1, 2-2, 2-3 and 2-4 were taken by Jerry Bourne, a student in the Material Science Department at the University of Florida. Figure 2-2 shows the microstructure of a conventional processed sample having the long striations or lines on the cut surface as pointed by arrows. These are called the alpha phase plates. The conventional processed sample shows that the alpha phase plates are bent at a smaller angle to the machined surface as compared to the advanced process sample and in this region of the surface they are nearly perpendicular to the machined surface.

By comparing the Figures 2-2 and 2-3 it is clearly visible that alpha phase plates are bent at a higher angle to the machined surface in the advance processed sample as compared with the conventional processed sample. The depth of this bent region appears to be 5 to 10 microns in the advanced process sample. Figure 2-4 shows the angle at which the alpha phase plates are bent at an angle to the machined surface. This bending

of alpha phase plates might be caused by the movement of cutting tool edge over the workpiece. This action of the cutting tool might cause plastic deformation which can further lead to the work hardening of the surface leading to the initiation of fatigue cracks thereby reducing the fatigue life.

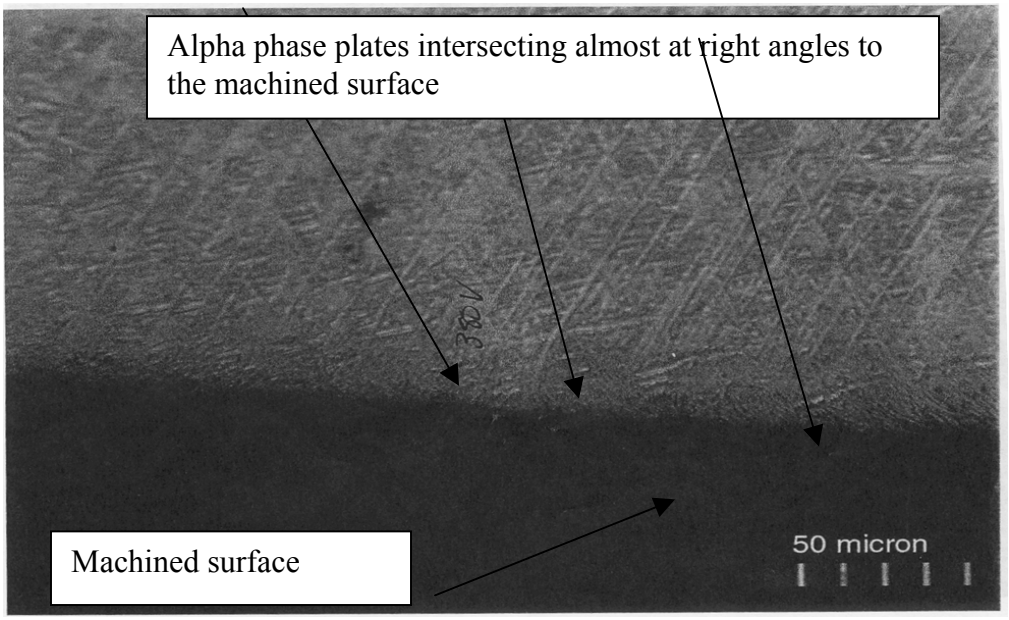

Figure 2-2 Microstructure of a conventional speed machined process sample

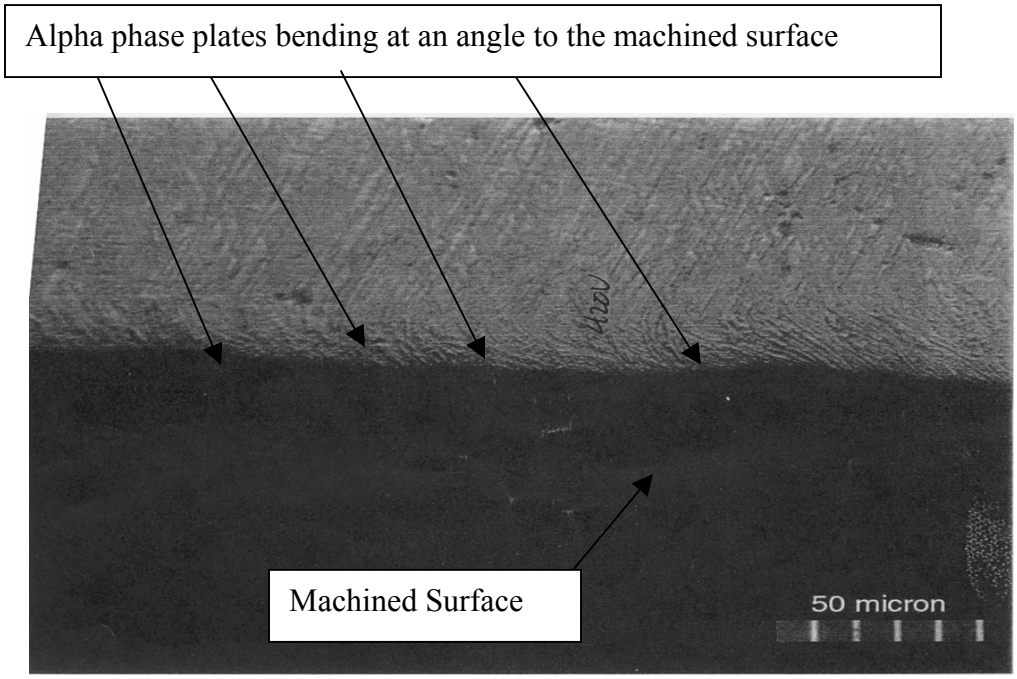

Figure 2-3 Microstructure of an advance speed machined process sample

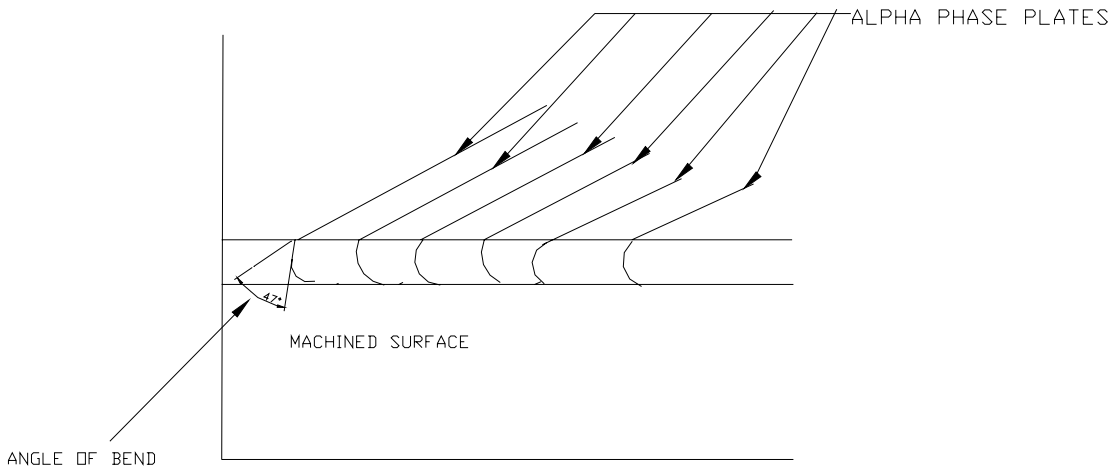

Figure 2-4 Plot shows the angle of bend at which alpha phase plates are intersecting to the machined surface

Figures 2-5 and 2-6 were also taken using optical microscope on the same surface but at a different location along the surface. The pictures show the surfaces at right angle to the machined surface. From the figures it is clear that the advance process sample has more surface defects as compared to the conventional processed sample as depicted by arrows. The size of these defects is of the order of 10 micrometers, making them able to act as stress concentrators and favorable sites for crack initiation.

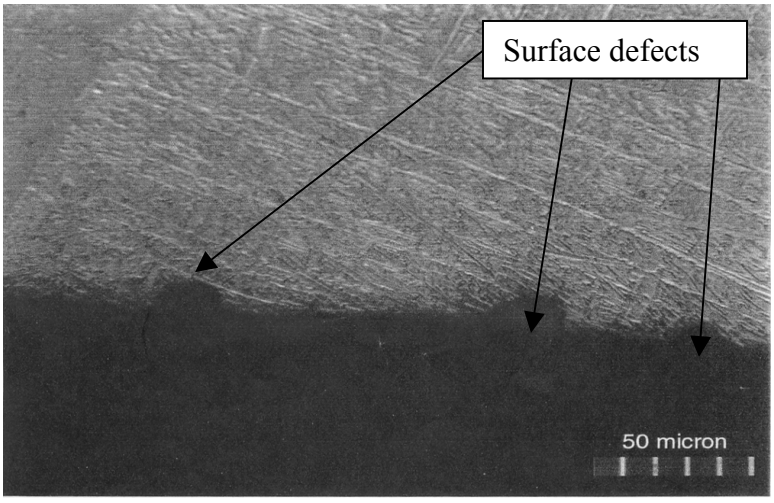

Figure 2.5 Microstructure of a sample machined using conventional process having surface defects

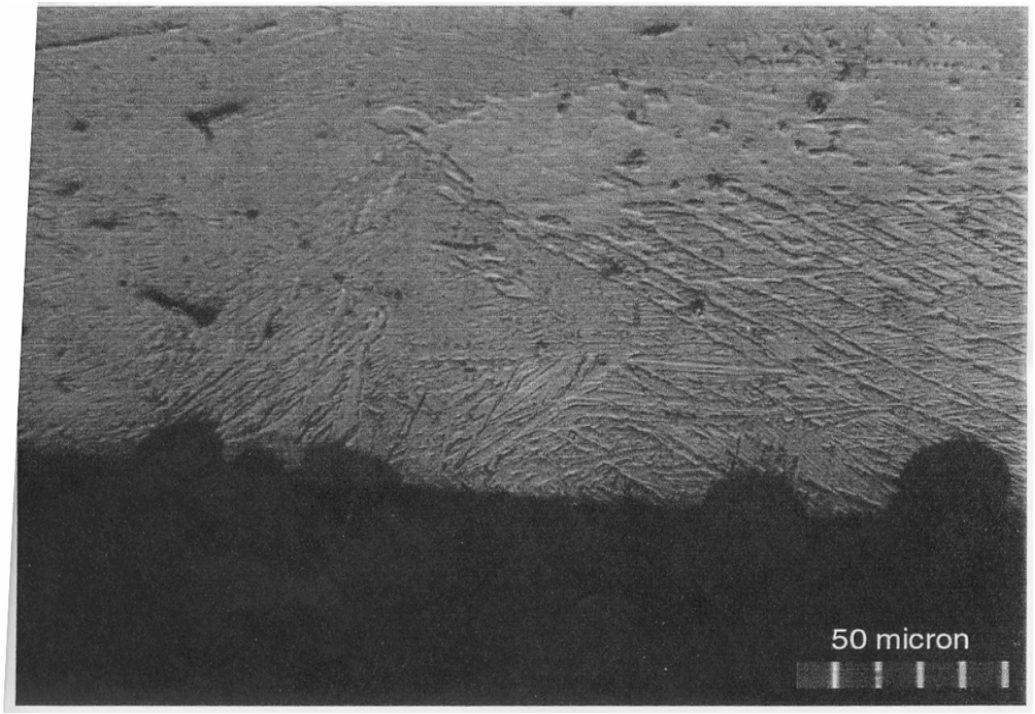

Figure 2.6 Microstructure of a sample machined using advanced process having more surface defects as compared to conventional process.

So, maintaining the surface integrity of Ti6Al4V after high speed and conventional speed machining is important especially when Ti6Al4V offers excellent properties due to which this alloy finds its applications in a wide range of industries like aerospace, marine, power generation and biomedical [8]. The defects seem to occur more in advance speed machined specimens than in conventional speed machined specimens. Also the machining processes can result in the plastic deformation of the top layer of the Ti6Al4V surfaces which can act as areas of higher stress leading to the earlier initiation of fatigue cracks thereby affecting the properties of the material. This behavior of plastic deformation is more pronounced in advance speed machined specimens as compared with the conventional speed machined specimens. After observing the figures of advance and conventional machined specimens, it seems that the damage due to advance and

conventional machining processes appears to be in the top layer of the machined surface and the thickness of this layer is very low

Machining tests were done on Ti6Al4V workpieces to determine the possible changes that advance speed machining process and conventional machining process could cause on the surface topography of Ti6Al4V. These machining tests are discussed in Chapter3

CHAPTER 3
MACHINING TESTS

Machining tests were done at the Machine Tool Research Center (MTRC) to simulate similar parameters to those used at BHT (Bell Helicopter Textron). The operation used at MTRC for the cutting tests was the face-milling operation. The following cases discuss the cutting parameters used to machine the workpieces using conventional machining process and advance machining process.

3.1 Case 1: Conventional machining process

In face milling the depth of the layer removed is axial depth of cut a_a and the width of the cut workpiece is the radial depth of cut a_r [3]. The workpiece was mounted on the tombstone using the clamps. The tombstone is a square cross section block made of cast iron mounted on the rotary table of the machine. Initially the workpiece was machined using the cutting parameters given in Table 3.1 for a full immersion case but the spindle stalled during the cut as the spindle did not have the required torque. The required peak torque came out to be more than the available torque from the spindle of Ingersoll (machine tool used for carrying out the cutting tests). The torque-spindle speed and power-spindle speed characteristics of Ingersoll are given in Figures 3.2 and 3.3. In order to get similar chip formation and heat generation, the axial depth of cut was required to be maintained as 0.125 inch. So, calculations were done for the peak torque by varying the radial depth of cut but keeping the same axial depth of cut and it was found that for a 60% radial immersion cut the peak torque came out to be 29.48 N-m which was less than the available torque from the spindle. The calculated cutting parameters for the 60%

radial immersion case are given in the Table 3-1.The first column of the table shows the type of machining parameters used, the second column shows the machining parameters used for machining the coupons at Bell Helicopter Textron (BHT) and the third and fourth columns show the parameters used for machining the workpieces that were calculated at (MTRC) for a full immersion and for 60% radial immersion cases. The parameters were calculated by simulating the same surface speed as was used by BHT (104 sfm). Surface speed is the linear speed at which the cutting edge moves over the surface of the workpiece. Surface speed is calculated by using the equation:

$v = n \pi D_{eff}$ [3]

where v = surface speed, n = spindle speed, D_{eff} = effective diameter

The calculations for the cutting parameters given in Table 3-1 were done using the following formulae given by equations (3-1), (3-2), (3-3) and (3-4) [3].

$$\text{Average Torque } T = \frac{P \times 60}{2*\pi*n} \tag{3-1}$$

where T = torque (N-m), P= power (W), n= spindle speed (rpm)

$$P = \frac{MRR \times K_s}{60} \tag{3-2}$$

where MRR = Metal removal rate(cm^3/min), K_s = Specific force (N/mm^2)

$$MRR = 0.001 \times f \times a_a \times a_r \tag{3-3}$$

where a_a = axial depth of cut (mm), a_r = radial depth of cut (mm)

$f = m \times n \times c$ (3-4)

m = number of teeth, c = chip load (mm)

In Table 3-1 Ti6Al4V coupons were machined at BHT and the workpieces were machined at MTRC

The following program was written in Matlab for determining the peak torque.

```
%Program for determining the variation of torque in the milling for a 60% radial
immersion case [3].
    m=4;                                %given number of teeth
    fis=0;                              %starting angle fis
    RI=60;                              %given percent radial immersion
    fie=(pi/2) + asin(1-2*((100-RI)/100))    %calculation of exit angle fie
    dfi=pi/180;                         %taken dfi = 1 degree
    Ks=2000;                            %given Ks = 2000 N/mm^2
    b=0.125*25.4;
    c=0.004*25.4;
    FX(1)=0;                            %initialize
    FY(1)=0;                            %initialize
    F(1)=0;                             %initialize
    Torque(1)=0;                        %initialize
    Fx=zeros(720,m);                    %creates a 720 x m array of zeros
    Fy=zeros(720,m);                    %creates a 720 x m array of zeros
    for n=1:720                         % seek results over two cutter revs i.e.720 degrees
    sumx=0;                             %initialize dummy x-force variable
    sumy=0;                             %initialize dummy y-force variable
    for i=1:m                           %forces to be summed over all teeth
    fi(n)=n*dfi;                        %angular position of leading tooth
    ang(n)=fi(n)*180/pi;                %amount of cutter revolution in degrees
```

```
al=fi(n)-(i-1)*2*pi/m;              %angular position of every tooth in turn
if al<fis                           %tooth has not entered the cut yet
elseif al>fie & al<(2*pi+fis)       %tooth exits cut and has not entered again yet
elseif al>fie+(2*pi)                %tooth exits cut again
Fx(n,i)=0;                          %Fx = 0 as tooth is not in cut
Fy(n,i)=0;                          %Fy = 0 as tooth is not in cut
else                                %tooth is engaged in the cut
Fx(n,i)=(Ks*b*c)*(sin(al)*cos(al) + 0.3*sin(al)^2);
Fy(n,i)=(Ks*b*c)*(sin(al)^2 - 0.3*sin(al)*cos(al));
end
sumx=sumx + Fx(n,i);                %increments Fx
sumy=sumy + Fy(n,i);                %increments Fy
end
FX(n)=sumx;                         %Cumulative x-force as cutter steps forward
FY(n)=sumy;                         %Cumulative y-force as cutter steps forward
F(n)=sqrt(FX(n)^2 + FY(n)^2);       %cumulative total force as cutter steps forward
Torque(n)=F(n)*(38.1/1000);
end
Fsum(1)=0;
for q=2:720
Fsum=Fsum+F(q);
end
Favg=Fsum/720;
```

```
Fpeak=max(F(n));

Torqueavg=Favg*(38.1/1000)

Torquepeak=Fpeak*(38.1/1000)

figure (1)

plot (ang,Torque,'-k')

grid on

xlabel ('ang (deg)')

ylabel ('Torque(N-m)')

gtext('Ks=2000 N/mm^2, 4 teeth')

gtext('chipload 0.1016 mm (0.004"), axial depth 3.175 mm (0.125")')

gtext('modeled as straight tooth cutter')

title ('Variation of Torque in Milling the Ti-6Al-4V alloy on the HVM60A')
```

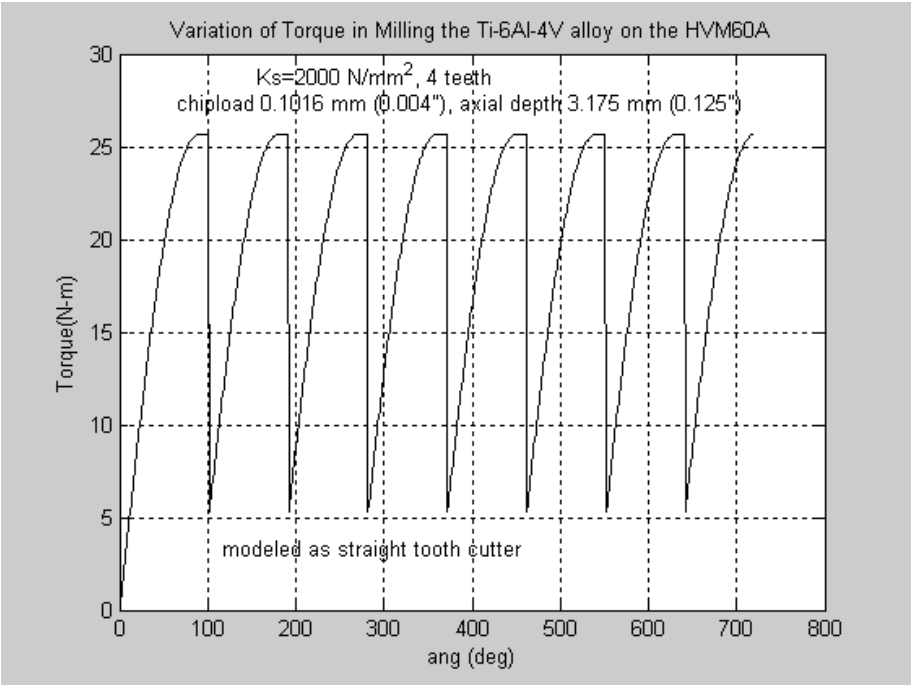

Figure 3-1 Variation of torque in milling Ti6Al4V alloy for 60% radial immersion

Table 3-1 shows different values of cutting parameters calculated using full and 60% radial immersion cases. The calculation for the cutting parameters shown in Table 3-1 were done using equations (3-1), (3-2), (3-3), and (3-4). The values for the peak torque were recorded from the plots obtained from the programs written in Matlab for different radial immersion of cases.

Table 3-1 Cutting parameters calculated for a conventional process

Parameter	**Coupons machined at BHT**	**Workpieces machined at MTRC**	
Type of immersion	Full	60% RI	Full
Diameter of cutter (inch)	4	3	3
Number of inserts	6	4	4
Axial depth of cut (inch)	0.125	0.125	0.125
Chip load (inch)	0.008	0.004	0.004
Feed rate (inch /min)	2.4	2.128	2.128
Spindle speed (rpm)	100	133	133
Specific Force (N/mm^2)	2000	2000	2000
M.R.R (cm^3/min)	19.66	7.846	13.07
Power (W)		261.53	435.89
Surface Speed (sfm)	104	104	104
Average Torque (N-m)		18.78	31.24
Peak Torque (N-m)		25.66	98.31

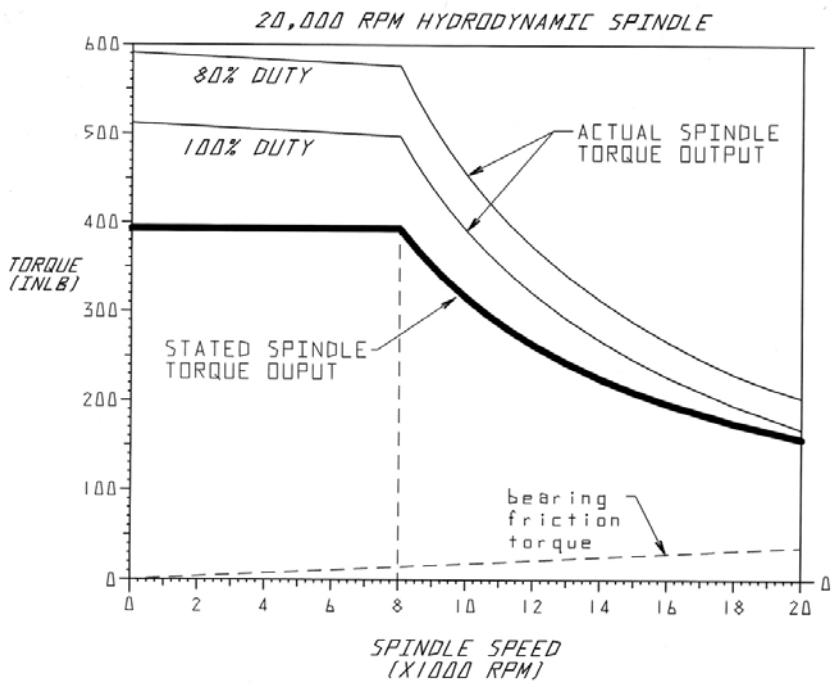

Figure 3-2 Torque-Speed characteristics of the Ingersoll HVMM [19]

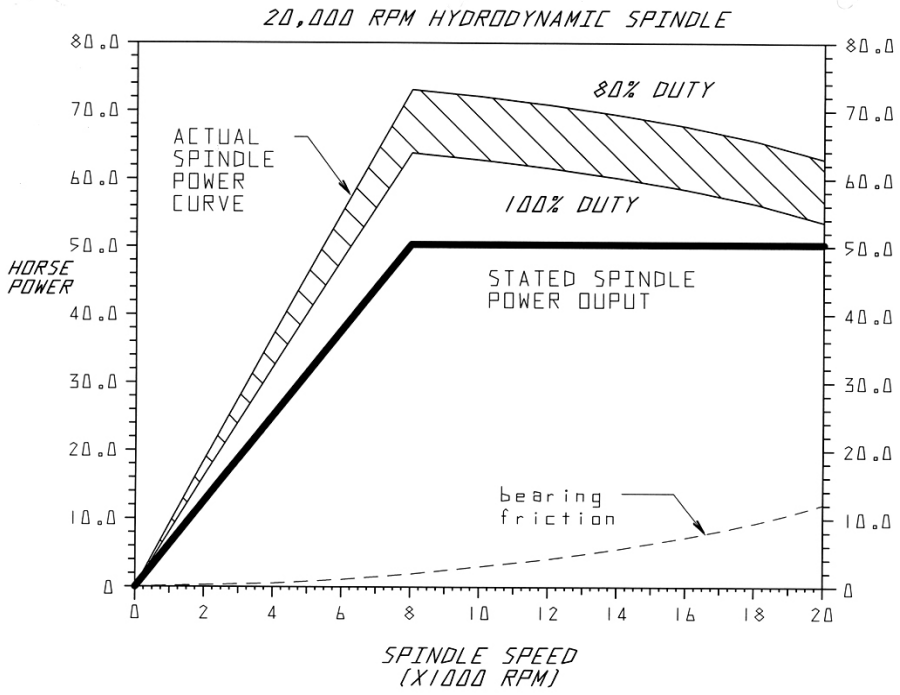

Figure 3-3 Power-Speed characteristics of the Ingersoll HVMM [19]

Figure 3-4 shows the workpiece machined using cutting parameters given in Table 3-1. The arrow points towards the machined area.

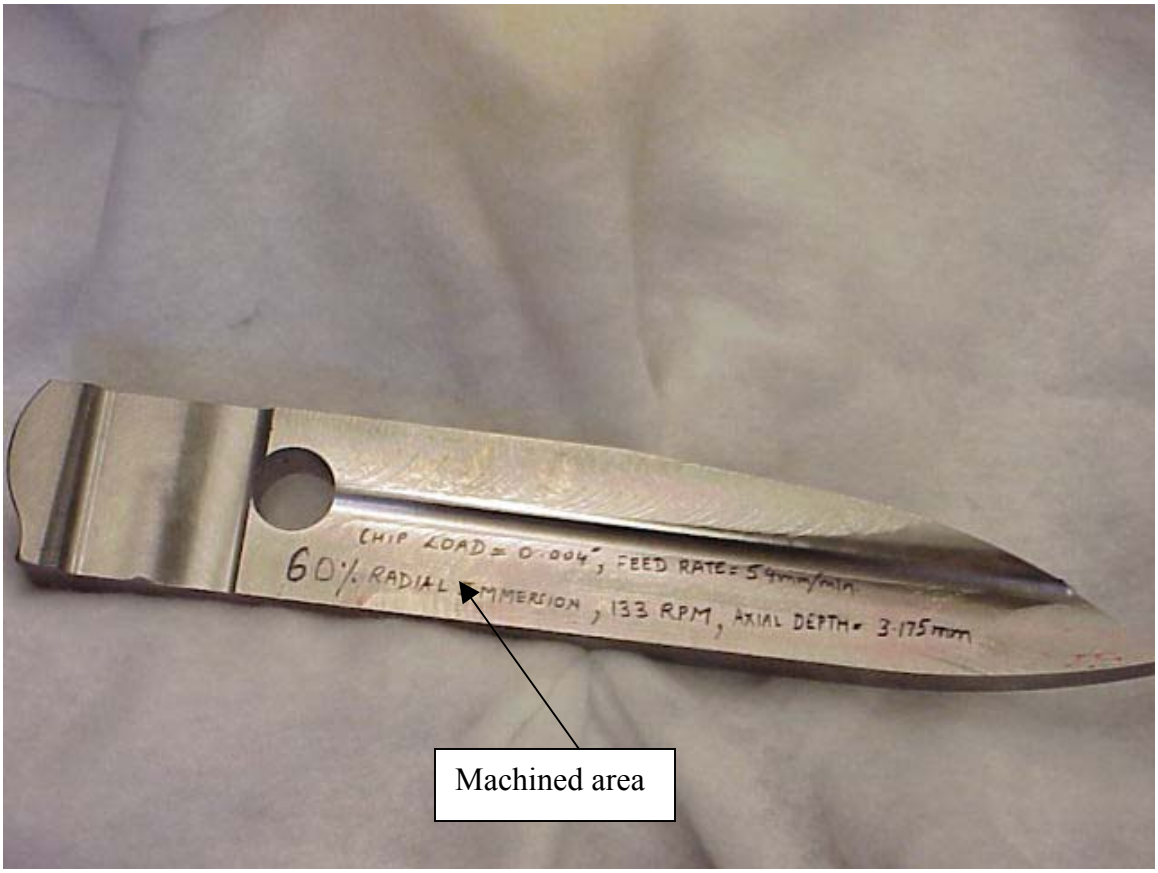

Figure 3-4 Workpiece machined using cutting parameters at MTRC given in Table 3-1 for a 60% radial immersion case

3.2 Case 2: Advance Machining Process

Several machining tests were conducted at UF by Chris Martin to find the optimum parameters for machining Titanium alloy Ti6Al4V. These tests can be found in [6]. Tests for tooling selection for the same cutting parameters can be found in [13].Table 3-2 shows the cutting parameters that were calculated at MTRC for various radial immersion cases. These parameters were calculated by simulating the same surface speed used at BHT (209 SFM) for the advance speed process. As the peak torque calculated at MTRC

came out to be 98.31 N-m which was far more than what is available from the spindle of the Ingersoll, the desired axial depth of cut of 0.125 inch could not be made using full immersion. Calculations were done with different radial depths of cut and was it found that the peak torque calculated using 40% radial immersion would be 39.31 N-m which was less than the available torque from the spindle. A single machining pass was then made on the workpiece with 40% radial immersion and with 0.125 inch axial depth of cut at a speed of 266 rpm with a feedrate of 8.51 inch/min.Similarly other areas were machined on the same workpiece using different radial depths of cuts as shown in Table 3-2. Figure 3-4 shows the machined workpiece in which arrow #1 points towards the area machined using 40% radial immersion. Arrow #2 points towards the area machined using 30% radial immersion. The specifications of the machine tool used for doing the cutting tests is given in Chapter 5.

Machining was also done using a special set of parameters to see the effect of 500 rpm spindle speed and low axial depth of cut of 0.078 inch on the cut surface. The machining operation was a slotting operation. The surface machined with this set of parameters is marked by the arrow #3 in Figure 3-5.

Another workpiece made of Ti6Al4V was machined using the advance machining parameters and then a finish machining pass was made on the workpiece.
The finish machining pass was made using 0.5mm as the axial depth of cut and at a spindle speed of 512 rpm using a feedrate of 54mm/min. on half of the machined area that was machined using advance speed machining parameters while a slow finish machining pass was made on the other half at 266 rpm. The reason for doing these finish

machining passes was to see the changes on the surface topography by adopting different spindle speeds.

Same axial depth of cut of 0.5mm was used for the finish machining pass on the other half of the advance speed machined area The chip load used for the finish machining passes was 0.004 inch.

Table 3-2 Cutting parameters used for the advanced process

Parameter	**Coupons**	**Workpieces machined at MTRC**				
Type of immersion	Full	30% RI	40% RI	50% RI	Full immersion	
Diameter of cutter	4	3	3	3	3	
Number of inserts	6	4	4	4	4	
Axial depth of cut (inch)	0.125	0.125	0.125	0.125	0.125	
Chip load (inch)	0.008	0.008	0.008	0.008	0.008	
Feed rate (inch/min)	6.5	8.51	8.51	8.51	8.51	
Spindle speed (rpm)	200	266	266	266	266	
Specific Force (N/ mm^2)	2000	2000	2000	2000	2000	
M.R.R (cm^3/min)		15.68	20.91	26.14	52.30	
Power (W)		523.07	697.26	870.18	1743	
Surface Speed (ipm)	209	209	209	209	209	
Torque (N-m)		18.78	25.04	31.31	62.62	
Peak Torque (N-m)		29.48	39.31	49.15	98.31	

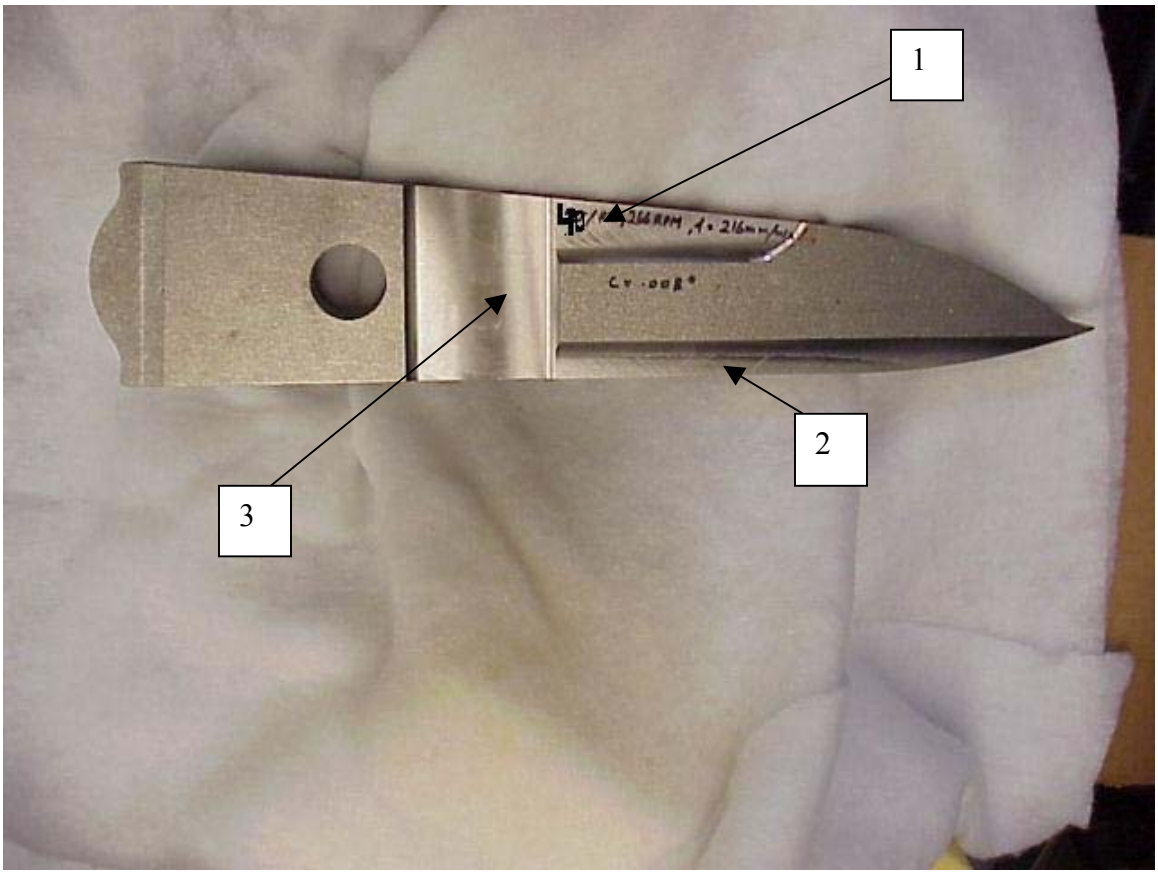

Figure 3-5 Workpiece machined using cutting parameters given in Table-3.2

3.3 Problems during cutting tests

Cutting Ti6Al4V can be dangerous as the chips can catch fire [13]. Initially cutting tests were tried on another high speed milling machine known as HSM1 at the machine tool research center. This machine is a 5 axis CNC machine with a spindle power of 36 KW and spindle speed of 36000 rpm. This machine has a single nozzle for the coolant spray. The cutting process had to be discontinued in order to avoid the sparks which came out during the interaction of the inserts with the titanium material. So flood coolant was used during the cutting tests as the coolant covers the whole chip area and reduces insert heating during the machining operation. The heating of the inserts is a big problem while machining Ti6Al4V as the cutting tool heats up quickly due to the low diffusivity of heat

into the workpieces and chips while milling. The reason is that Ti6Al4V has a low thermal conductivity of 7.2 W/m·K (BTU/ft.h·°F) [2] so heat does not dissipate easily from the tool chip interface resulting in the high temperatures of the tool. Ti6Al4V has high chemical affinity meaning that it has high tendency to react with many other elements so the chemical reaction takes the material out of the cutting tool thereby weakening it [13]. Since most cutting tool materials react with Ti6Al4V, the choice of the cutting tools is limited. Also the high temperatures in milling Ti6Al4V tend to increase the affinity making the problem worse. So proper care should be taken while selecting cutting tools for machining Ti6Al4V [13].

The second problem that arose while machining the workpieces was with using the vise as the work holding fixture instead of the tombstone. Due to the low stiffness of the vise, the workpiece was not able to sustain the high chip loads commanded during machining, so the workpiece chattered.

Chatter is a self- excited type of vibration that occurs in metal cutting if the chip width is too large as compared with the dynamic stiffness of the system. Under these conditions vibrations start and quickly grow. The cutting forces become periodically variable reaching considerable amplitudes, the machined surfaces become undulated and the chip thicknesses varies so much that the surface becomes dissected. Chatter is easily recognized by the noise associated with these vibrations and by the chatter marks on the surface. So, chip width and metal removal rate should be kept below the limit at which chatter occurs [3]. Figure 3-6 shows the workpiece that was machined using the vise as the work holding fixture. The chatter marks can be seen on the machined surface marked with an arrow. The part was held horizontally in the vise and the machining pass was

made from negative X axis to positive X axis at a feedrate of 8.51 inch/min using 0.125 inch as the axial depth of cut. The cut was made with a face mill of 3 inch diameter at a spindle speed of 266 rpm. This case was a 40% radial immersion case.

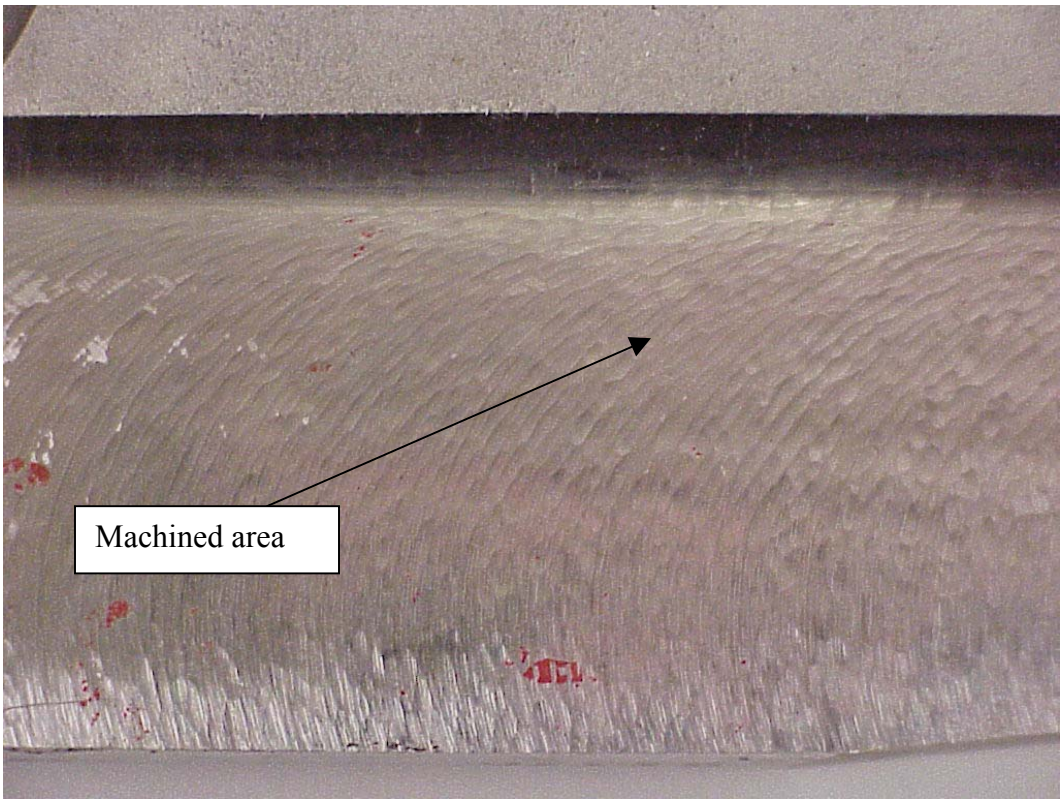

Figure 3-6 Workpiece showing chatter marks on the machined surface

Figure 3.6 shows another workpiece machined using the vise as the work holding fixture. This workpiece was machined using 30% radial immersion. The feed rate was maintained at 8.51 inch/min and axial depth of cut as 0.125 inch. A 3 inch diameter face mill was used at a spindle speed of 266 rpm. The chatter marks can be easily seen on the machined surface in Figure 3-7. So rigidity of the workholding fixture plays an important role in maintaining the surface integrity of the parts especially with titanium, where the

work has the tendency to deflect under tool pressures due to the low modulus of elasticity of titanium

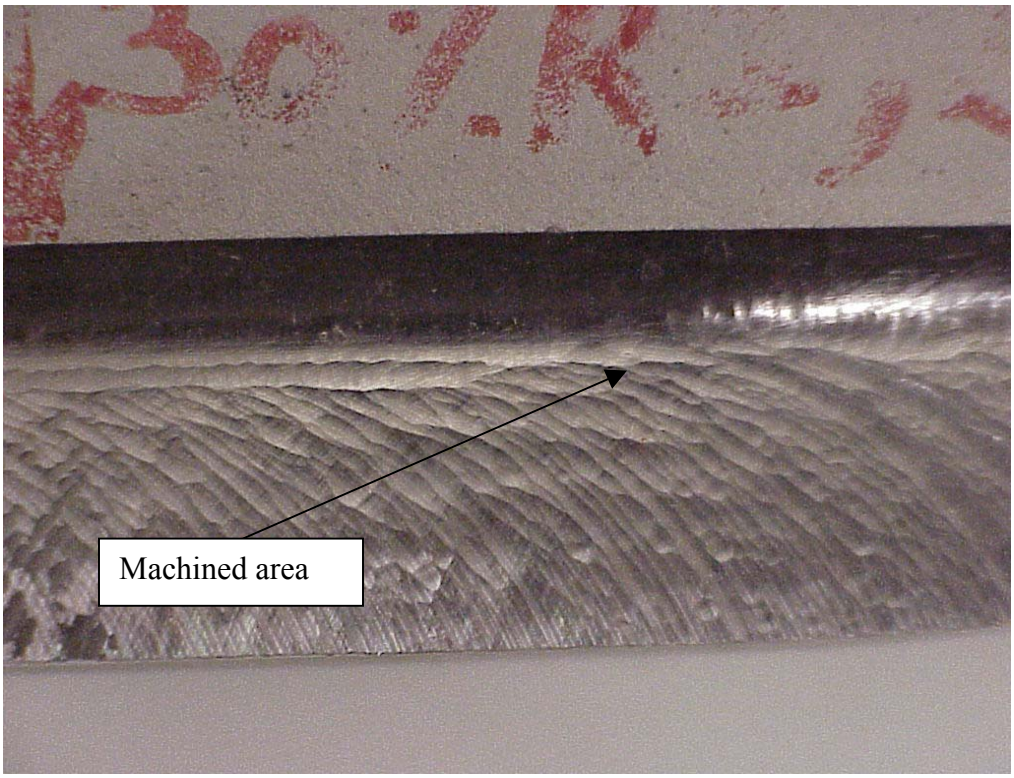

Figure 3-7 Workpiece showing chatter marks on the machined surface

.

After the workpieces were machined they were sent to TRIAD EDM Inc. (Dunnellon, FL) for the wire EDM cuts. The specimens were cut out from each of the 3 different machined areas using wire EDM for the microstructural analysis which is discussed in Chapter 4.

CHAPTER 4
MICROSTRUCTURE ANALYSIS

Observing the microscopic structure of materials reveals characteristics that have a tremendous influence on their technological utility. Some of the features that contribute to the strength of materials, and virtually all of the features that initiate mechanical failure, are resolved by optical microscopy. Thus, preparation of optical microscopy specimens, their observation using optical microscopes, and interpretation of photographs taken with optical microscopes (micrographs) play a vital role to understand the origin of material properties. In this chapter various operations that were performed for preparing the specimens, detailed microscopic study and the hardness tests that were done on the Ti6Al4V specimens are discussed.

4.1 Preparation of Metallographic Specimens

The objective of preparing metallographic specimens was to reveal the structural features so that they can be observed and possibly measured. The first step was to prepare a highly polished surface, and the second step was to chemically or electrochemically attack the surface in a way that would reveal the grain boundaries. Each of these steps involved many separate operations. These individual operations are discussed in the following section in the order they were performed.

4.1.1 Cutting of the specimens

Since the workpiece to be studied had large dimensions (19.5inch x 3.5inch x 1 inch) it was necessary to cut smaller pieces for metallographic study as it was difficult to polish larger cross-sections and maintain a flat plane of polish, so 4 slots of dimensions

(0.8inch x 0.8inch x 1.75 inch) and 2 slots with dimensions (1inch x 1inch x 1 inch) were taken out of the machined workpieces using wire EDM. The specimens were sent to TRIAD EDM Incorporation (Dunnellon, FL) for cutting out the desired slots. Since the cutting operation can generate substantial heat, it is important to recognize the close proximity of the material that is ultimately observed to the cut surface. The heat can change the microstructure so care must be taken to avoid over heating the specimen during cutting. Often, low speed saws are used to prepare the metallographic sections, so that heat treatment during the cutting operation is avoided. But due to low thermal conductivity and due to high specific strength of Ti6Al4V, wire EDM was selected for cutting. The principle on which wire EDM works is given as follows.

Wire EDM is a method to cut conductive materials with a thin electrode that follows a programmed path. The electrode is a thin wire. As the wire feeds from reel to reel, it uses sparks of electrical energy to progressively erode an electrically conductive work-piece along a path determined by the relative motion of the machine's axis. Typical wire diameters range from 0.004" - 0.012" although smaller and larger diameters are available. There is no physical contact between the wire and the part being machined. Rather, the wire is charged to a voltage very rapidly. This wire is surrounded by de-ionized water. When the voltage reaches the correct level, a spark jumps the gap and melts a small portion of the work piece. The de-ionized water cools and flushes away the small particles from the gap. Figure 4.1 shows the picture of the wire EDM cutting the part [15].

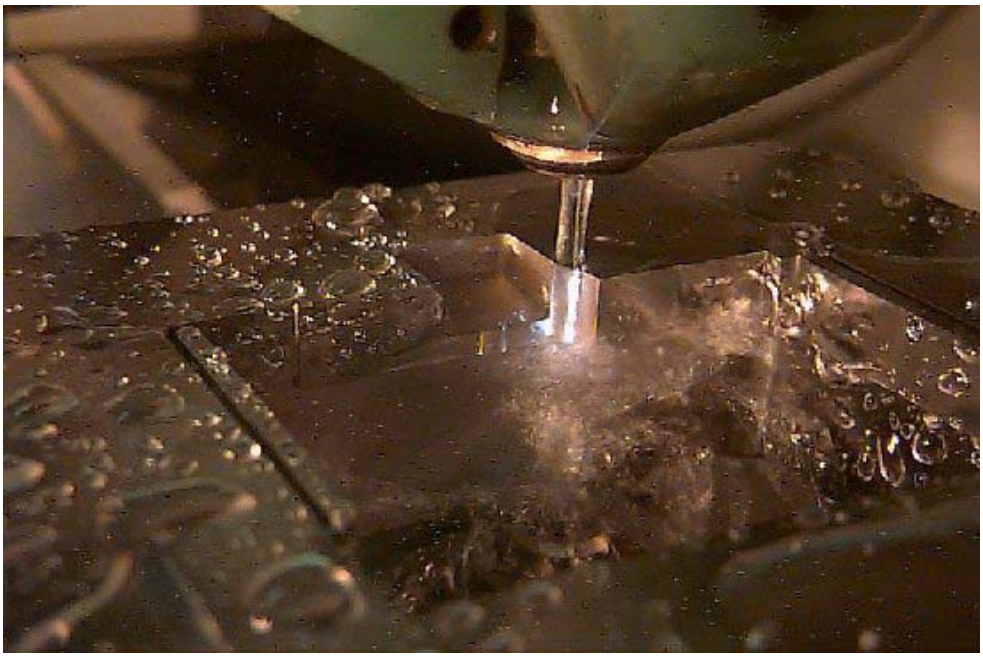

Figure 4-1 Wire EDM cutting the part (courtesy New Jersey Precision Inc.)

4.1.2 Grinding of the specimens

Grinding refers to abrasion of the specimen surface by coarse abrasive particles, which are usually either SiC or Al_2O_3 (corundum) bonded onto a heavy paper backing. A modest flow of water was passed to carry away the metal flakes grounded off the surface along with any grit particles that came loose from the grinding paper [16]. The abrasive particles are commonly specified in terms of grit size, with larger numbers indicating finer particles. The grit on each successive abrasive paper is finer than the grit on the previous paper. By proceeding through a series of successively finer grits, the scratched and damaged layers left by each grit size were removed by the next one. However, if the loose abrasive particles and metal flakes are carried from the previous grinding step to the new paper, the scratches won't get any finer. For example, if grit is carried from the 240 paper to the 400 paper, some of the scratches left after the 400 grit grinding step will be

produced by the 240 grit particles. For this reason, it was essential to wash the specimens when changing grit sizes.

The grit sizes that were used for grinding process were 240, 320, 400, and 600. The number is related to the sieving process that separates the abrasive particles into different sizes. For example, the 320 grit particles means that all particles that get passed through a wire mesh sieve with 320 fine wires per inch. The openings in a 320 mesh sieve are about 25 microns square and any abrasive particle that passes through a 320 mesh sieve can be used on 320 grit abrasive paper [16]. Table 4-1 below shows the standard grit sizes used for grinding with the size of the grits in microns.

Table 4-1 Standard grit sizes used [16]

GRIT NUMBER		
European (P-grade)	Standard grit	Median diameter, (microns)
P240	240	58.5
P320	280	46.2
P400	240	35
P600	400	25.75

The objective of each grinding step was to remove the scratches and damaged layer left behind by the previous step. If 240 grit abrasive paper was used first, then jumped to 600 grit, it would have taken a long time for the very fine abrasive particles on the 600 grit paper to abrade away the thick scratched and damaged layer left by the 240 grit paper. So instead of jumping from the 240 grit to the 600 grit paper directly and spending a long time at the 600 grit step, it was decided to pass the specimens through

each of the intermediate grit sizes: 240,320, 400, and then 600, spending only a short time grinding with each one. The method described below gave consistent results [16].

1. When changing to a finer grit size, the specimen was rotated 90^o from the scratch orientation left by the previous step, and ground until all previous scratches were gone. This eradicated the scratches left from the previous coarser grit.

2. The specimen was then again rotated $90^o$and continued with the same grit size until the scratches from step 1 were gone. This was enough to eradicate the damaged layer left under the surface by the previous coarser grit.

3. The specimens were then switched to next finer grit size and started again from the step 1.

4.1.3 Polishing of the specimens

Polishing refers to abrasion of the specimen surface by fine abrasive particles, which are usually suspended in water or another solvent [16]. In this case a small amount of the solution containing the abrasive particles was poured onto a cloth. The billiard cloth was used for the polishing of the Ti6AlV specimens. The cloth was stretched over a flat wheel that was rotated at 200 RPM. The specimen was held against the spinning wheel. This was done to bring the cloth containing the abrasive particles in contact with the specimen. The abrasive particles that were used in the slurry put on the cloth were of aluminum oxide (Al_2O_3) though a wide variety of abrasive particles can be used, for example diamond (C), magnesium oxide (MgO), and iron oxide (Fe_2O_3) [16].

The specimens were initially polished using the slurry made of alumina (Al_2O_3) with suspension sizes of 15 micron. The next step was to polish the specimens with slurry having suspension size of 5 micron. Then the specimens were polished using the slurry having suspension size of 1 micron and finally using 0.3 micron.

4.1.4 Chemical etching of the specimens

The final result of the grinding and polishing operations was a smooth mirror-like surface. Observing this surface in the microscope often revealed little about the microstructure of the material. Smaller particles and other features such as grain boundaries were invisible after the polishing step. These grain boundaries should be allowed to reflect light differently than the primary phase, so that they can be distinguished in the microscope. The method used involved chemical etching of the polished surface, which is described below.

Considering the surface topology effect when materials are dissolved in a solvent, atoms or molecules are removed from the solid and enter the solvent. This general picture of dissolution is equally valid for metal dissolving in an acid or a molten salt, or for a polymer dissolving in a solvent such as acetone. The solvent must break the atomic bonds that hold the atoms or molecules in the solid, and allow them to escape into the solvent. Clearly, the strength of the bond that holds the atom or molecule in the solid affects the rate of dissolution [16]. For atoms in the center of a grain or in the crystalline phase of a semi crystalline polymer, the interatomic forces are the characteristic of the crystal and the dissolution rate is approximately constant for specific conditions. For atoms near grain boundaries, the local atomic arrangement is different from the ideal arrangement in the crystal [16]. It is reasonable to suppose that atoms or molecules in these special locations are not as strongly bonded to the solid as atoms or molecules within the crystals. Therefore, more rapid dissolution from a metal surface can be expected where grain boundaries and dislocations emerge at the polished surface. This is the reason why the grain boundaries are etched for any polycrystalline material.

The specimens were etched using Kroll's reagent. The composition of this etching solution that was used for Ti6Al4V is as follows [16]:

Deionized water (DI): 100ml

Hydrofluoric Acid (HF): (40%): 3ml

Nitric Acid (HNO_3) (1.4): 6ml.

The etching time was 3-10 seconds. Grain boundaries have high energy spots and etching releases all the electrons, which are loosely held inside the atoms to reveal the microstructure [16].

4.2 Metallographic analysis under optical microscope

After polishing and etching, metallographic specimens were ready for observation.

Specimen # 1 and 2 are the conventional machined specimens.

Specimen # 6 and 7 are the advanced machined specimens.

Specimen # 5 and 8 are the specimens which were machined by using a special set of parameters to see the effect of 500 rpm spindle speed and low axial depth of cut of 0.078 inch on the cut surface.

4.2.1 Surface Defects

An optical microscope was used to analyze the surface of the specimens. The description of the microscope and the procedure adopted for taking observations has been discussed in Chapter 5. Figures 4-1, 4-2, 4-3, 4-4 and 4-5 show the unetched surface of the advanced machined specimen taken at right angle to the machined surface of the advanced speed machined specimen #6. These pictures were taken at 5 different locations along the edge of the polished surface. These locations (#1, #2, #3, #4 and #5) were picked arbitrarily on the edge of the surface. The scale used is a 1mm scale and each division is of 10 microns. The magnification was 100x. The surface defects are clearly

visible on the edge of the surfaces and the depth of these defects range from as low as 10 microns to as large as 80 microns from the top of the surface to below the subsurface.

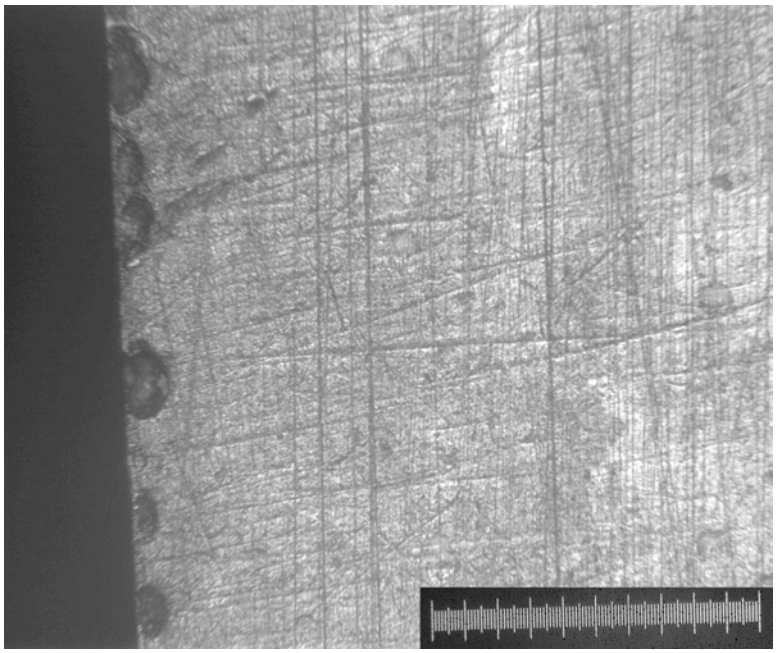

Figure 4-2 Microstructure of advanced machined process specimen#6 showing the defects caused by milling process at location #1 at magnification 100x

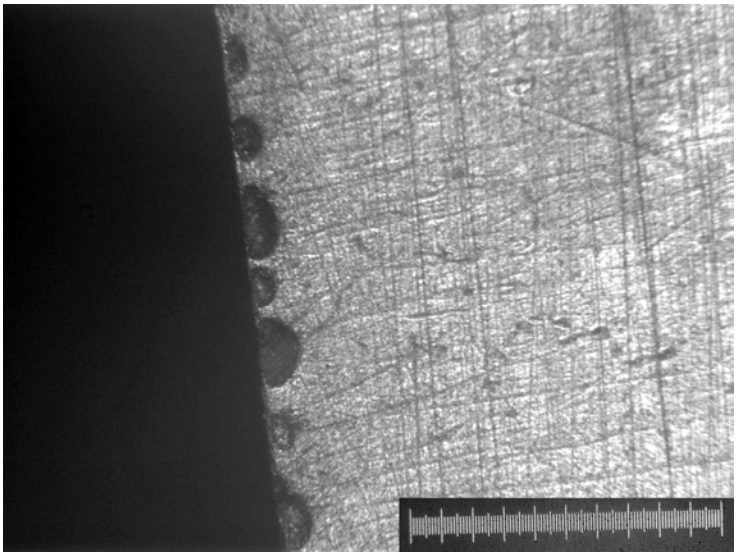

Figure 4-3 Microstructure of advanced machined process specimen#6 showing the defects caused by milling process at location # 2 at magnification 100x

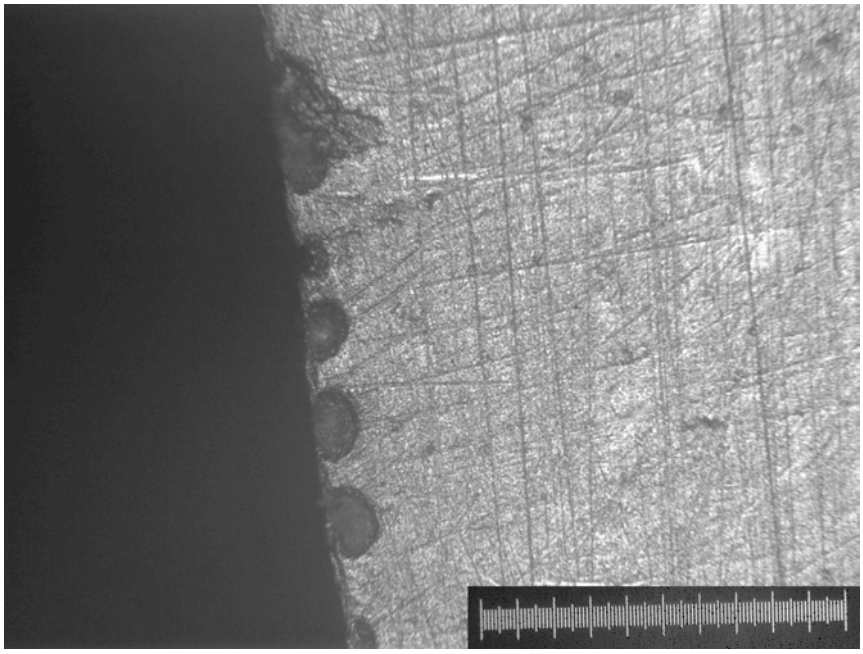

Figure 4-4 Microstructure of advanced machined process specimen#6 showing the defects caused by milling process at magnification 100x at location #3 on the surface

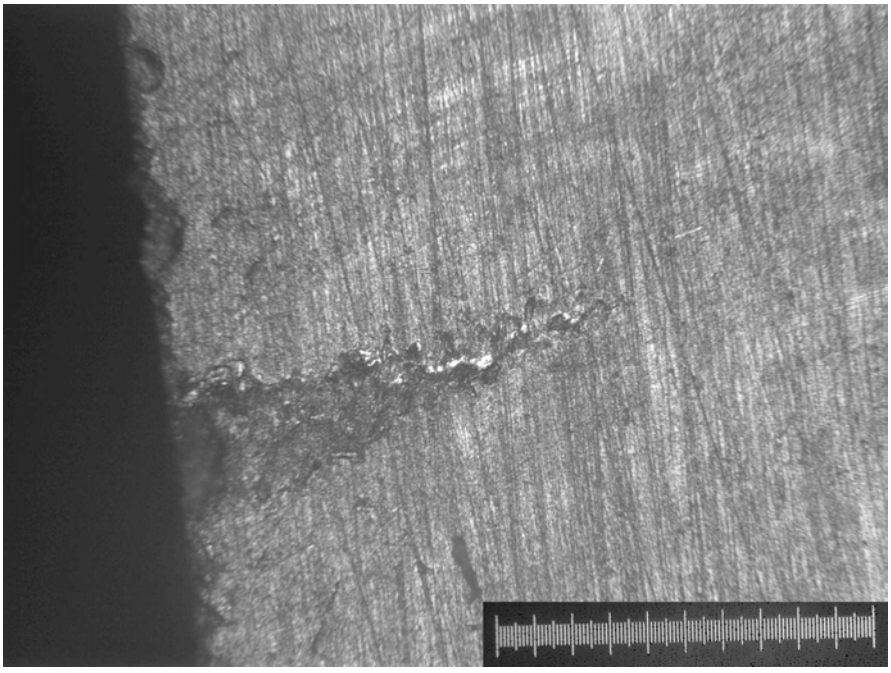

Figure 4-5 Microstructure of advanced machined process specimen#6 showing the defects caused by milling process at magnification 100x at location #4 on the surface

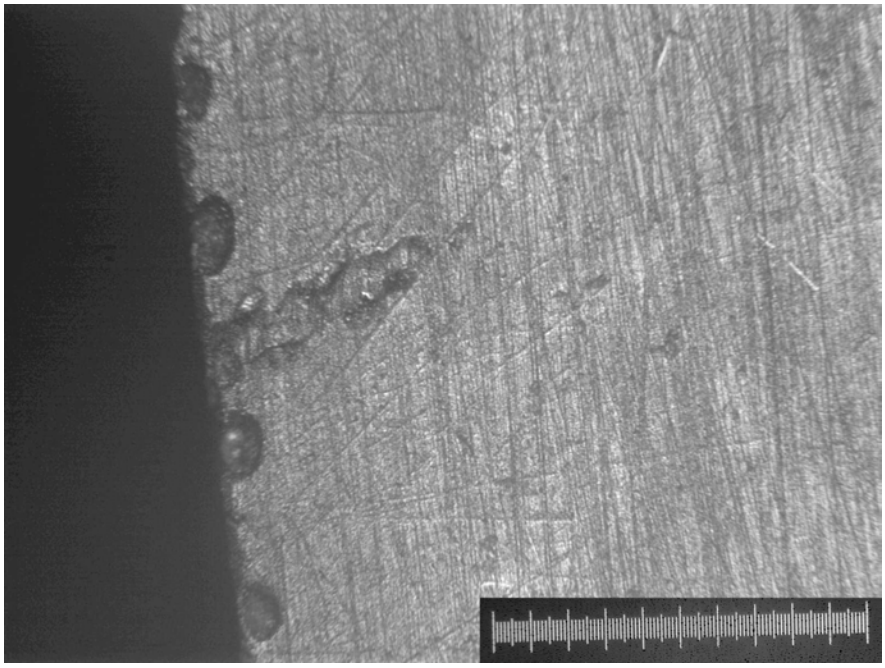

Figure 4-6 Microstructure of advanced machined process specimen#6 showing the defects caused by milling process at magnification 100x at location #5 on the surface

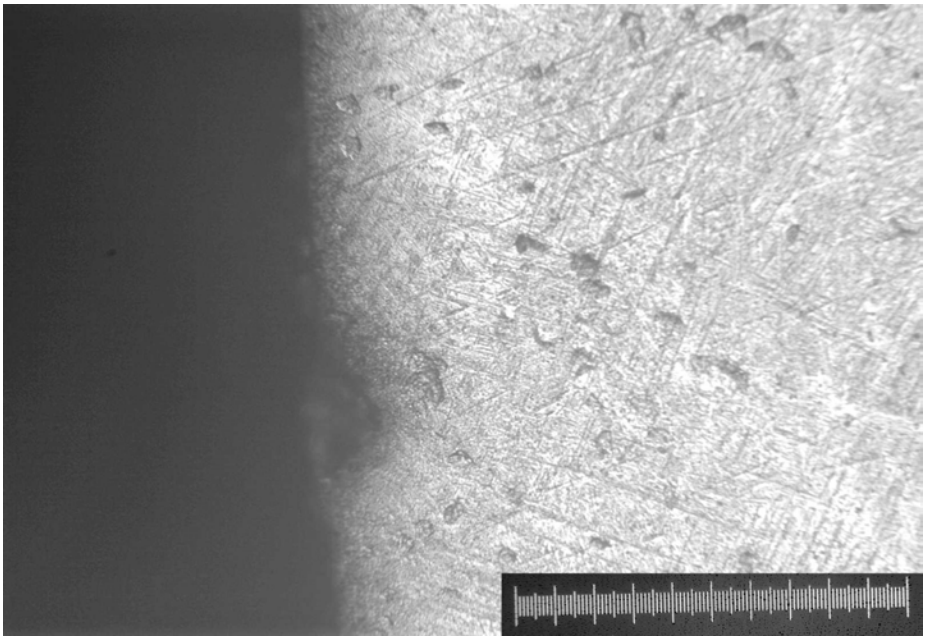

Figure 4-7 Microstructure of conventional machined process specimen#1 showing lesser number of defects at magnification 120x at location #1 on the surface

Figures 4-6 and 4-7 are the pictures taken by sectioning the specimens at right angle to the machined surface of the conventional speed machined specimens #1. These pictures were taken at 2 different arbitrary locations along the edge of the polished surface. The scale used is a 1mm scale and each division is 10 microns. The number of surface defects in the conventional machining case is less as compared to the defects in the high speed machining case. In conventional machining case the size of these defects may range from as low as 10 to as high as 60 microns from the top of the surface to below the subsurface.

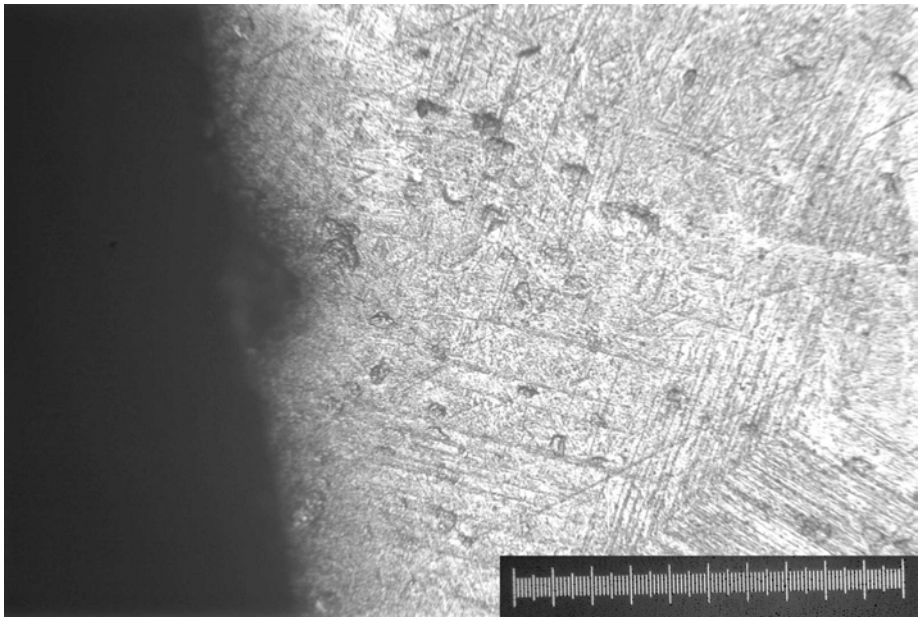

Figure 4-8 Microstructure of conventional machined process specimen#1 showing lesser number of defects at magnification 120x at location #2 on the surface

Figure 4-8 is the picture of the advance speed machined specimen #7 before it was etched. This picture was taken at an arbitrary location on the machined surface. It shows a large number of notches. The magnification was 50x. The arrow indicates the direction of machining. The scale shown in the picture is a 1mm scale.

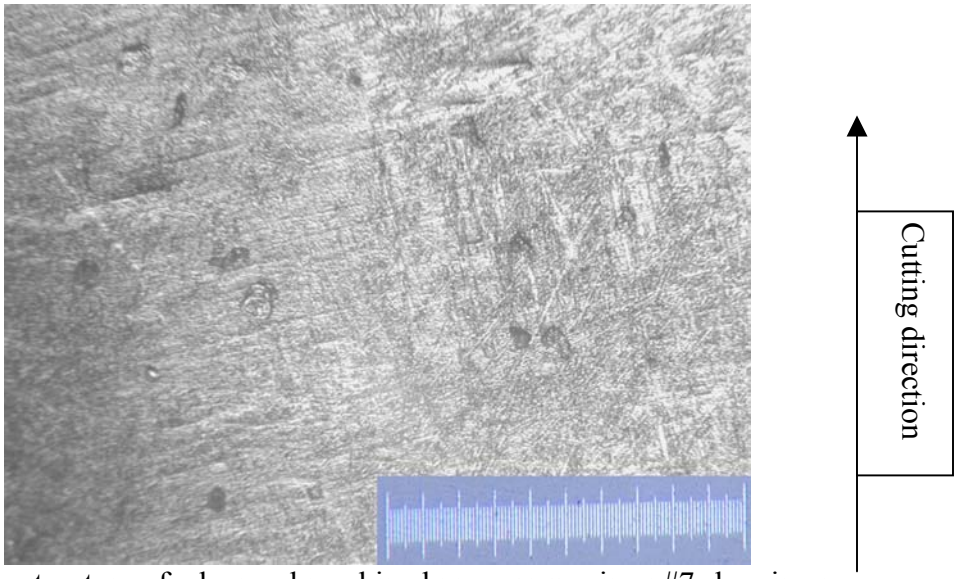

Figure 4-9 Microstructure of advanced machined process specimen#7 showing more number of notches at magnification 50 x

Figure 4-9 shows the picture of a conventional machined specimen taken on the machined surface of the specimen# 2. It can be noticed that the conventional machined specimen shows a lesser number of notches as compared to the high speed machined specimen. Figure 4-10 is the picture of the same specimen but at a different location and at a higher magnification of 150x.The scale used is a 1 mm scale.

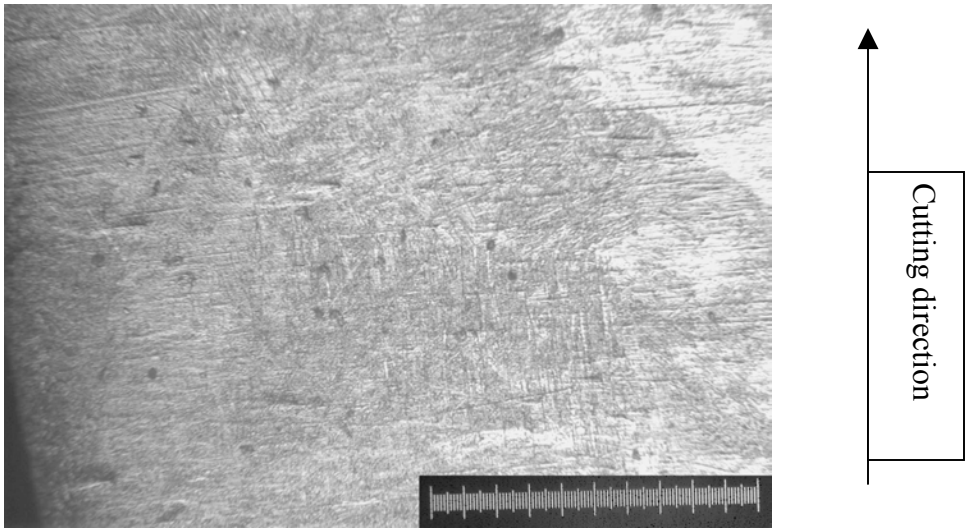

Figure 4-10 Microstructure of conventional machined process specimen #2 showing lesser number of notches at magnification 50x

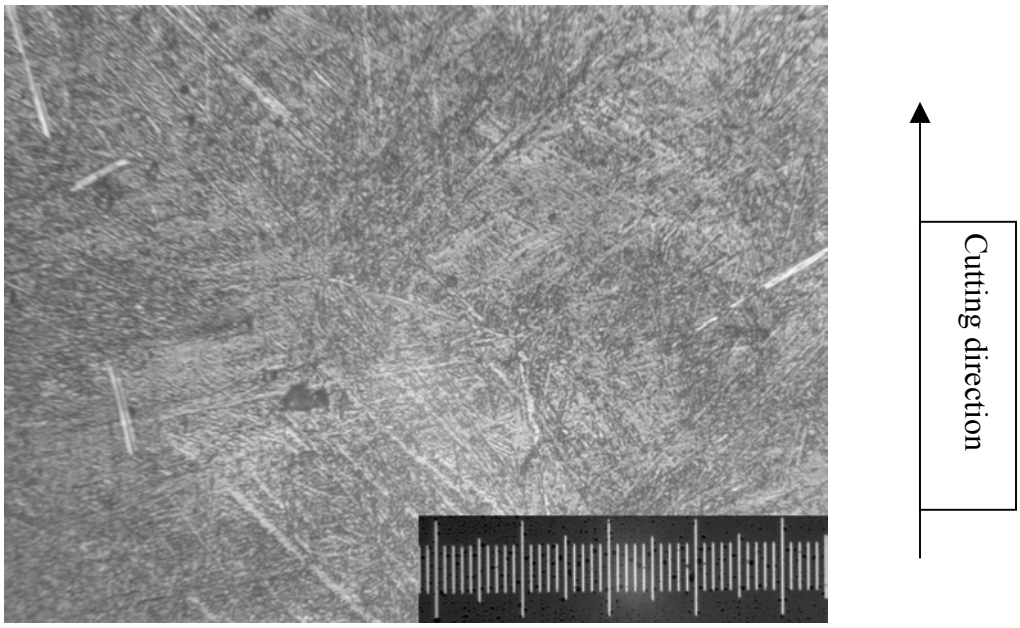

Figure 4-11 Microstructure of conventional machined process specimen #2 showing lesser number of notches at a higher magnification 150x

4.2.2 Microscopic analysis of grain sizes

The grain size is an important microstructural characteristic of Ti6Al4V as it has an important effect on the material properties. At low temperatures (less than 1/3 of the absolute melting temperature) grain boundaries strengthen materials. On the other hand, at high temperatures (above 1/2 of the absolute melting temperature), grain boundaries enable creep deformation to occur more rapidly [18].

To investigate the changes in the grain size, which might have been caused by the high speed and conventional speed machining processes, various pictures were taken on the machined surfaces Figures 4-11, 4-12, 4-13 and 4-14 show the distribution of grains in the microstructure of the specimens. The pictures shown in these figures were taken directly on the machined surfaces of the specimens.

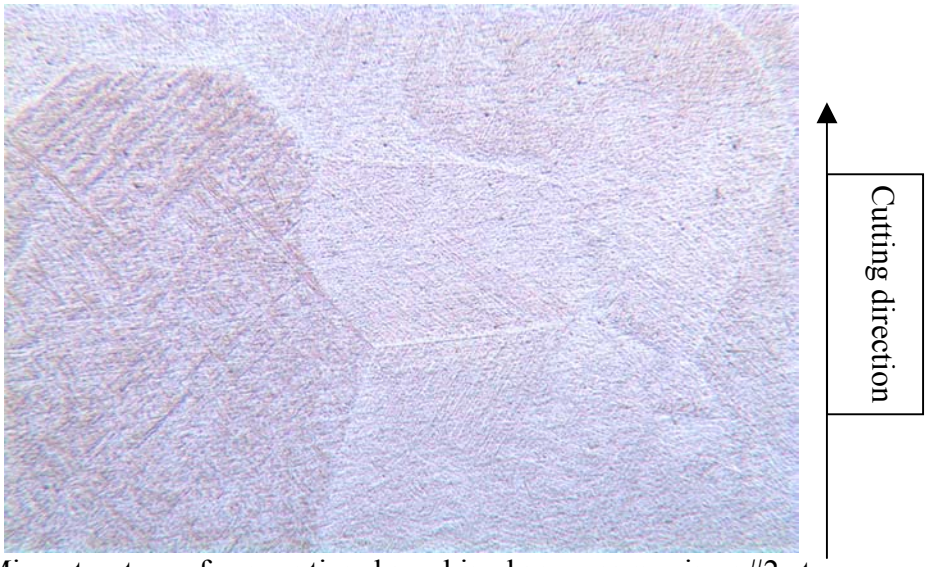

Figure 4-12 Microstructure of conventional machined process specimen#2 at magnification 80x

Figure 4-13 Microstructure of conventional machined process specimen #2 at magnification 120x

The light grains are the alpha grains while dark grains are the beta grains. The reason for this contrast is due to the difference in the reflectivity of alpha and beta phases during etching [16]. The reagent selected for etching the specimens was Kroll's reagent, which selectively attacks only the alpha phase [16], thus a contrast appears between the alpha and beta grains. Although certain information may be obtained from as-polished specimens, the microstructure is usually visible only after etching. Figures 4-11 and 4-12

show the grains in the conventional machined specimen #2.at an arbitrary location on the surfaces while Figure 4-13 shows the grains in the microstructure of an advanced process specimen #7 The defects formed on the machined surfaces of specimen #2 and specimen #7, due to the different machining processes, were removed during the grinding, polishing and etching processes before taking the pictures shown in Figures 4-11, 4-12 and 4-13.

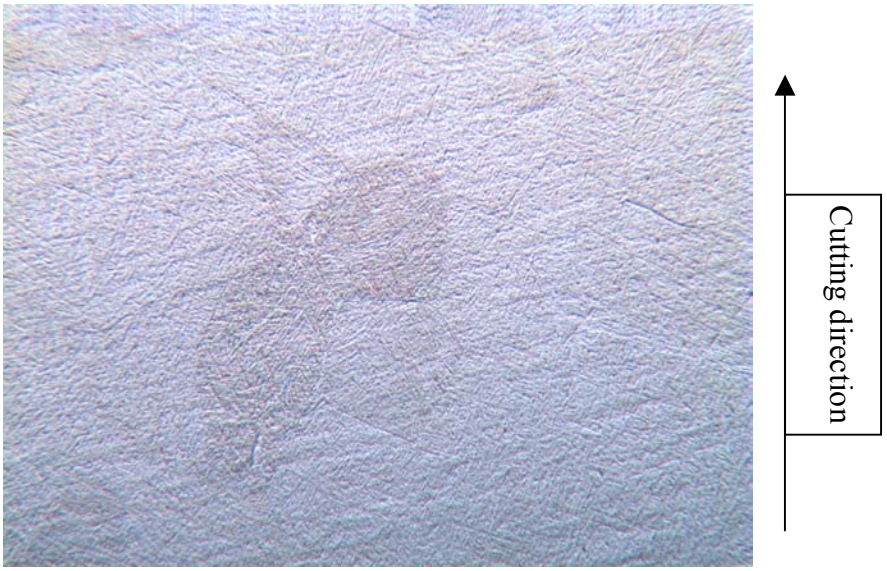

Figure 4-14 Microstructure of advanced machined process specimen #7 at 40x

In addition to showing the surface defects that were present in the microstructure, micrographs were used to make measurements of the grain size. The mean linear intercept method was used for measuring the grain size [16]. In this method a test line is marked on the micrograph as illustrated schematically in Figure 4-15 (a). The number of intersections of the line with grain boundaries is counted and used in the following formula:

D = Length of test line / (Number of intercepts x Magnification) (4-1)

where D = mean linear intercept grain size

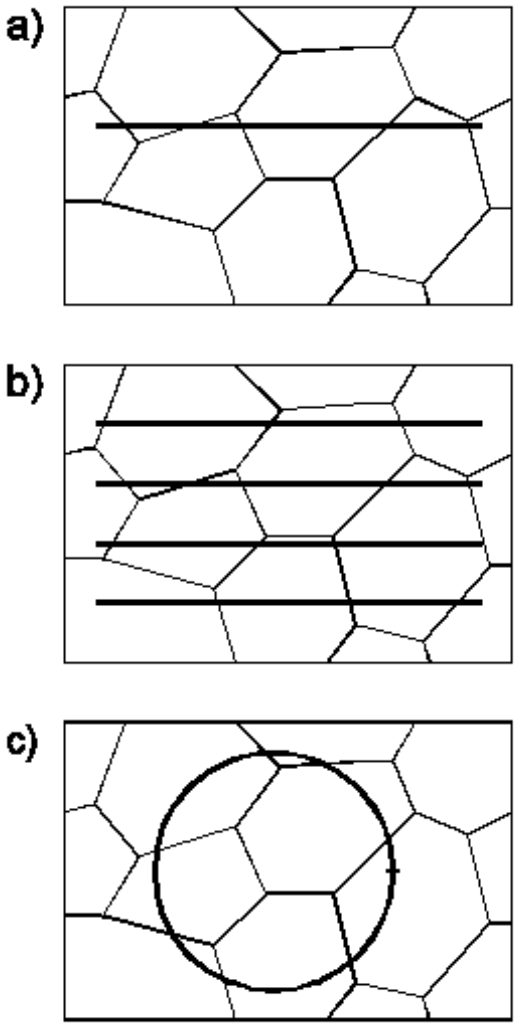

Figure 4-15 Illustration of the method used to measure the mean linear intercept grain size. a) A test line is marked on the micrograph. b) A longer test line is composed of several segments. c) A circular test line.

The test line placed in different locations produced different number of intercepts, resulting in a different calculated grain size. To make an accurate grain size measurement using this method, it was necessary to use a long enough line length so that large number of intercepts could be counted. In order to get large number of intercepts, it was not necessary to use a single line length rather a set of parallel lines as shown in Figure 4-14b could be used, or a circle as shown in Fig. 4-14c could be positioned over several

different micrographs in succession [16]. The grain size was determined by combining the total number of intercepts with the total line length using the equation (4-1).

The mean linear intercept grain size actually represents the average grain diameter in the plane of polish [16]. The average 3-D grain diameter is larger than the average diameter observed on the plane of polish because sometimes the plane of polish cuts through the widest part of the grain, but other times the plane of polish just cuts through the narrow tip of a grain as shown in Figure 4-15 [16].

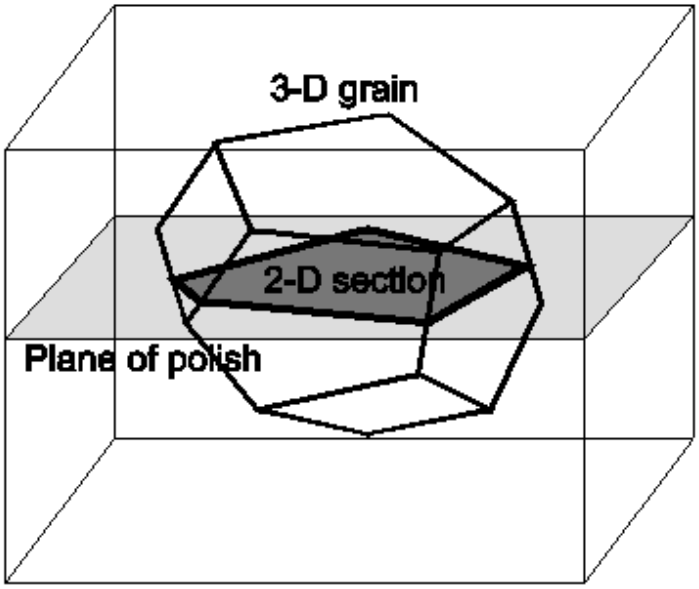

Figure 4-16. A polished and etched metallographic section actually represents a planar cut through a 3-dimensional structure of grain boundaries.

The grains of Ti6Al4V are equiaxed [2] and if the grains of a material are equiaxed (the same dimension in all directions), the true average grain diameter is about 1.6 times larger than the mean linear intercept grain diameter. [16].

An unmachined specimen of Titanium alloy (Ti6Al4V) was prepared for making a comparison of grain sizes between the machined and unmachined specimens. Then, a large number of parallel lines and circles were drawn on the micrographs of a high speed machined, conventional speed machined and unmachined specimen so as to obtain large number of intercepts. Calculations were done for true average grain diameters using equation (4-1) and it was found that the grain size of the high speed machined, conventional speed machined and the unmachined specimens came out to be approximately the same. The reason might be that the temperature produced during the high speed machining and conventional machining was not enough to change the grain size as the temperature required for the transformation of alpha to beta phase is 882 ^{o}C [2].

Figures 4-16 and 4-17 show the microstructure of the specimen #5 machined using a special set of machining parameters. The special set of machining parameters was:

- Axial depth of cut = 0.0787 inch
- Spindle speed = 500 rpm
- Feed rate = 2.12 inch / min
- Radial depth of cut = 3 inch

The microstructural analysis of specimen #5 shows very few notches on the machined surface, rather small pits were found. These pits as shown in Figures 4-16 and 4-17 are the result of abusive polishing and grinding processes. These pits cannot be the result of any of the machining processes as the size of these pits is very small as compared to the notches that were formed in the high speed machined and conventional speed machined specimens, shown in Figures 4-8, 4-9 and 4-10. The other point

supporting this effect is that the small pits did not appear on specimen #8, which was cut out from the same machined area Figure 4-18 shows the microstructure of specimen #8

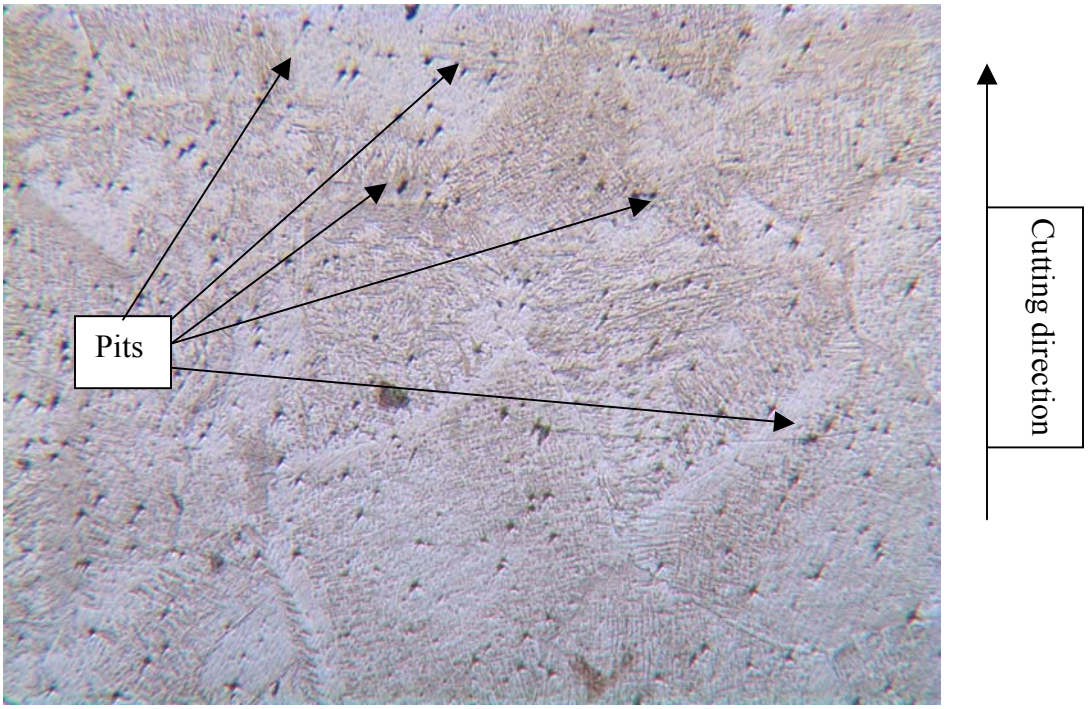

Figure 4-17 Microstructure of specimen# 5 at 80x showing pits

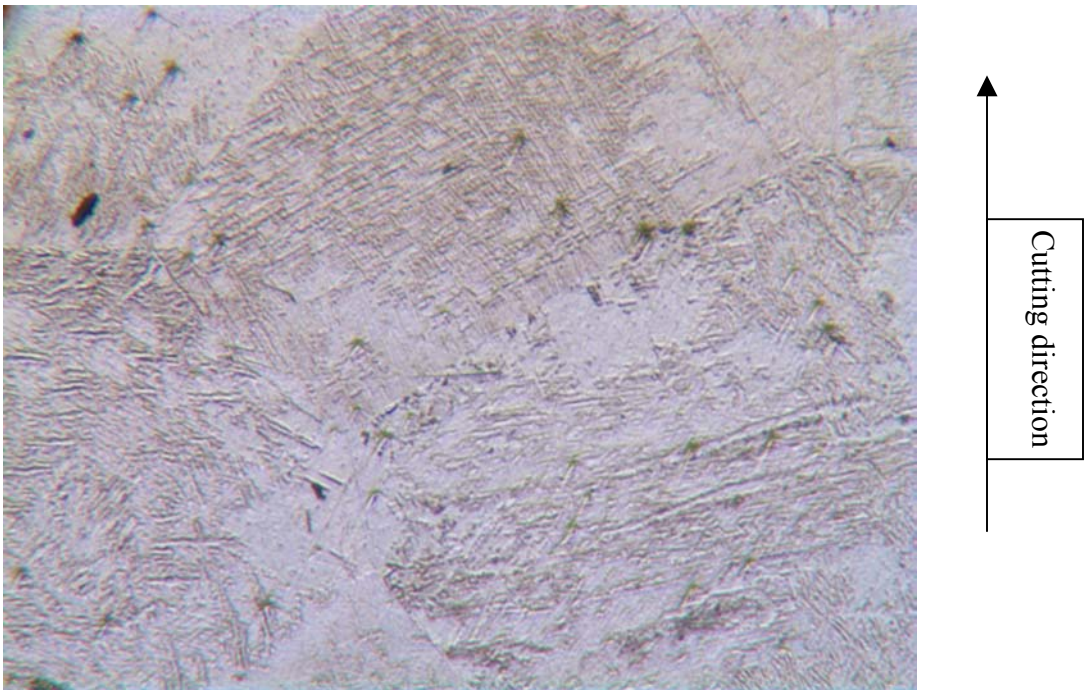

Figure 4-18 Microstructure of specimen# 5 at 120 x showing pits

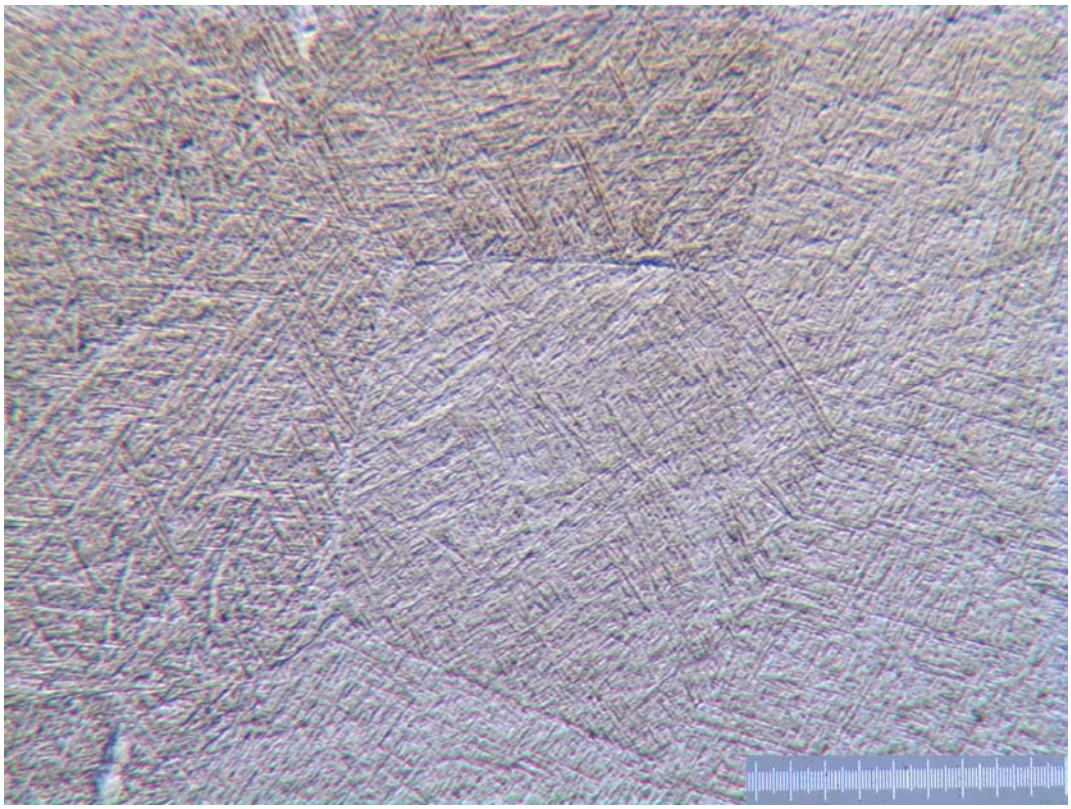

Figure 4-19 Microstructure of specimen# 8 at 120x

To investigate the location of the defects on the surface of Ti6Al4V and to study their interaction with the grain boundaries the following pictures were taken using optical microscope. Figures 4-20, 4-21, 4-22, and 4-23 were taken at right angle to the machined surface of a high speed machined specimen #6. These pictures were taken at 4 arbitrary locations along the edge of the surface at different magnifications. The surface defects are clearly visible along the edges of the cut surfaces. It is interesting to see that these defects lie inside the grains, i.e, they are a part of the grains and do not necessarily lie on the grain boundaries. Also it can be seen that the size of the grain is much bigger than the size of the defects. These defects are a part of the grains pulled out of the surface.

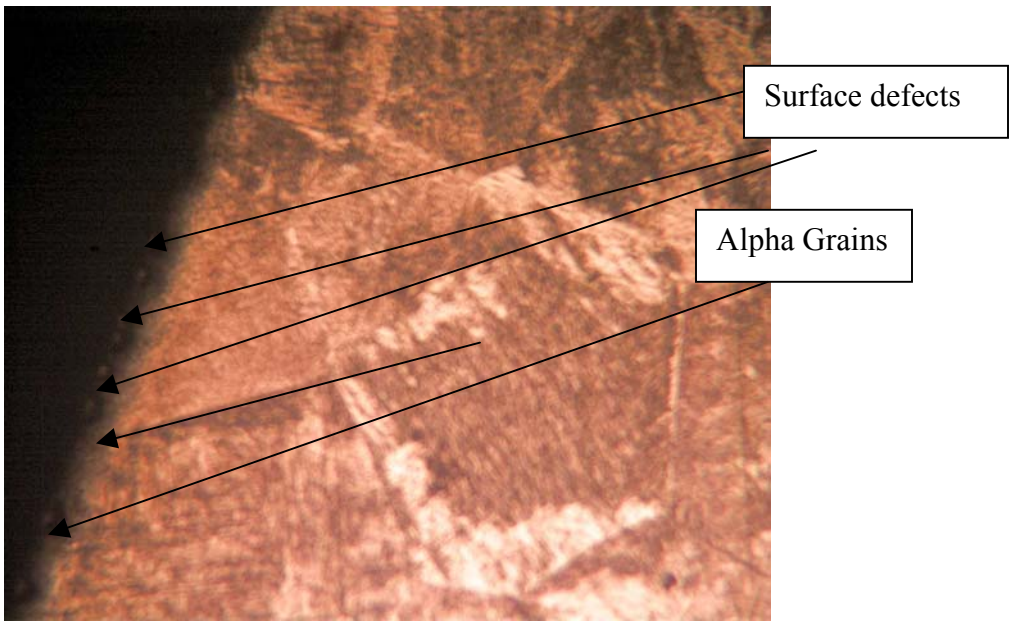

Figure 4-20 Microstructure of high speed machined specimen# 6 at 80x magnification at location #1 showing surface defects on the grains.

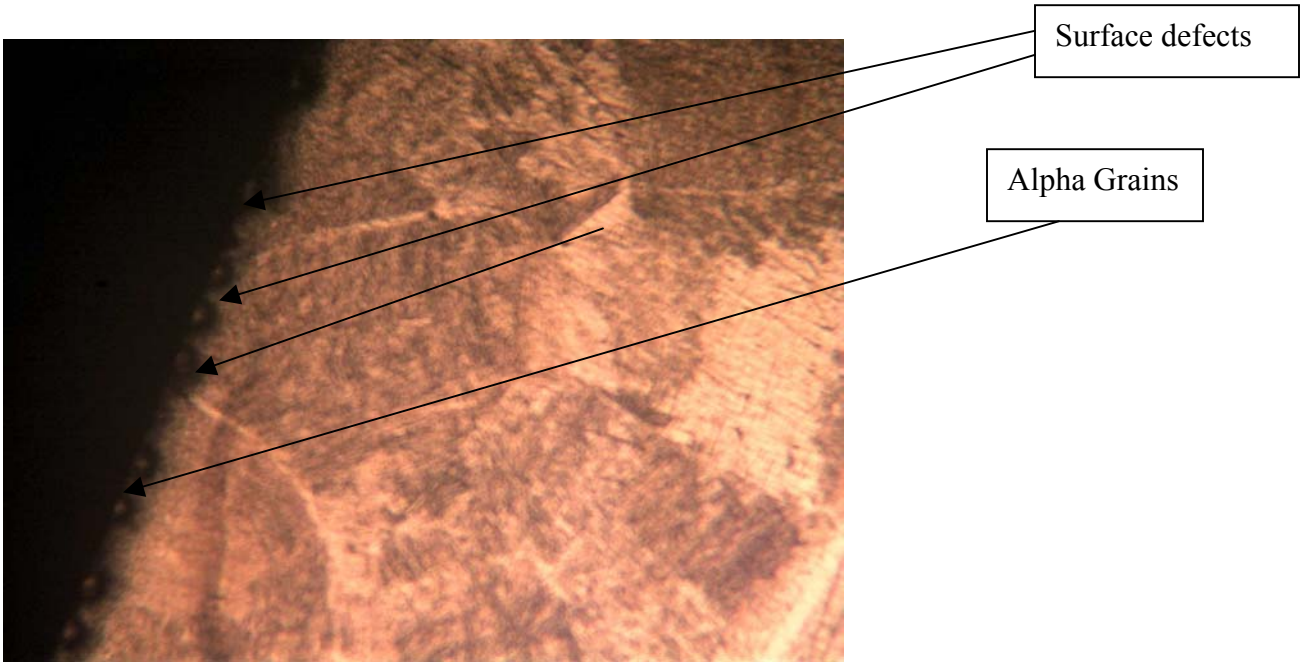

Figure 4-21 Microstructure of high speed machined specimen# 6 at 80x magnification at location #2 showing surface defects on the grains

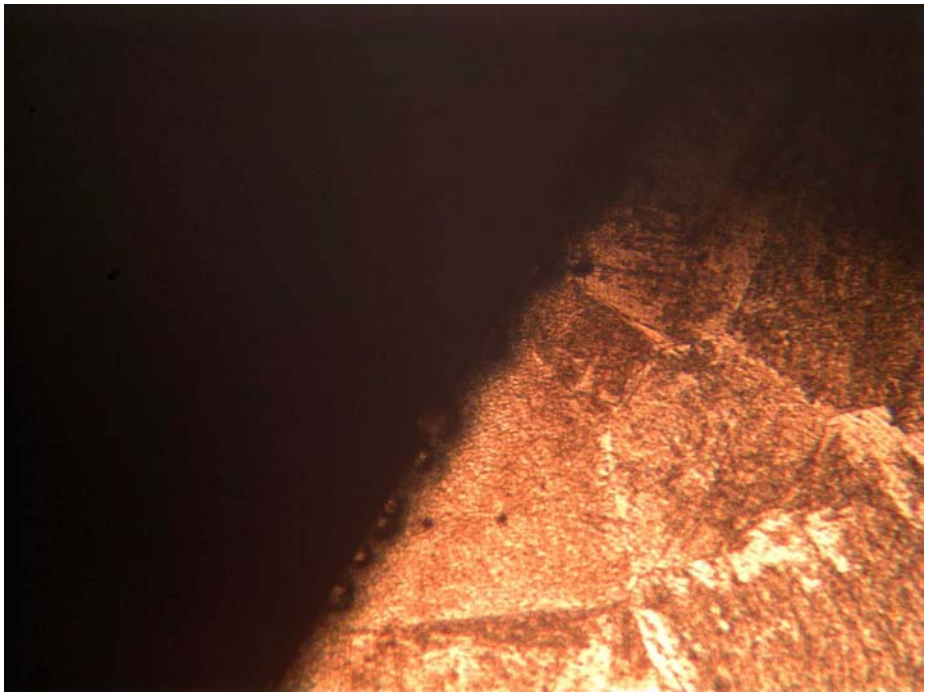

Figure 4-22 Microstructure of high speed machined specimen# 6 at 80x magnification at location #3 showing surface defects on the grains

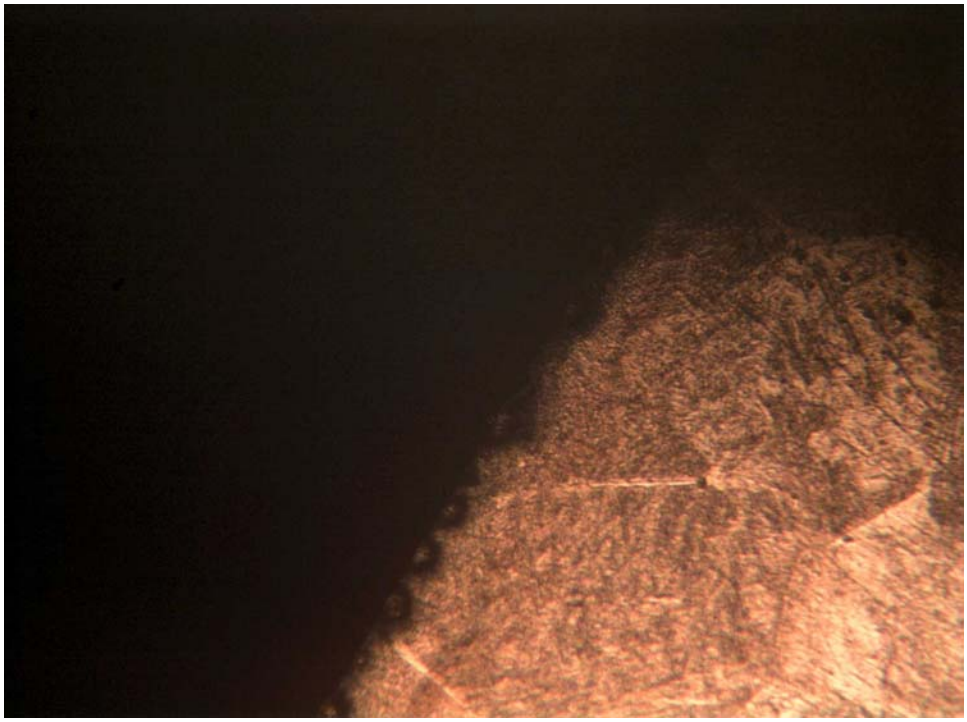

Figure 4-23 Microstructure of high speed machined specimen# 6 showing surface defects on the grains at 100x magnification at location #4

It has to be noted that at low temperatures grain boundary can act as a source of strength through resisting intragranular dislocation movement [16]. At high temperatures grain boundary is the source of weakness because it permits relative movement of one grain past another and also offers a preferred fracture path. These generalities can apply to fatigue [16].

4.2.3 Grain orientation

The pictures shown in Figures 4-23 and 4-24 were taken in order to investigate the effect of high speed machining and conventional speed machining processes on the grain orientation as misorientation effects, which result solely from the change in the crystal lattice, could occur [18]. By looking at the figures it can be noticed that all grains are oriented randomly and each crystal lattice or grain has its own definite direction of orientation. The temperature produced during high speed machining processes is not enough to orient the grains in a specific direction or a preferred direction so the grains are oriented in a random direction as visible in Figures 4-23 and 4-24.

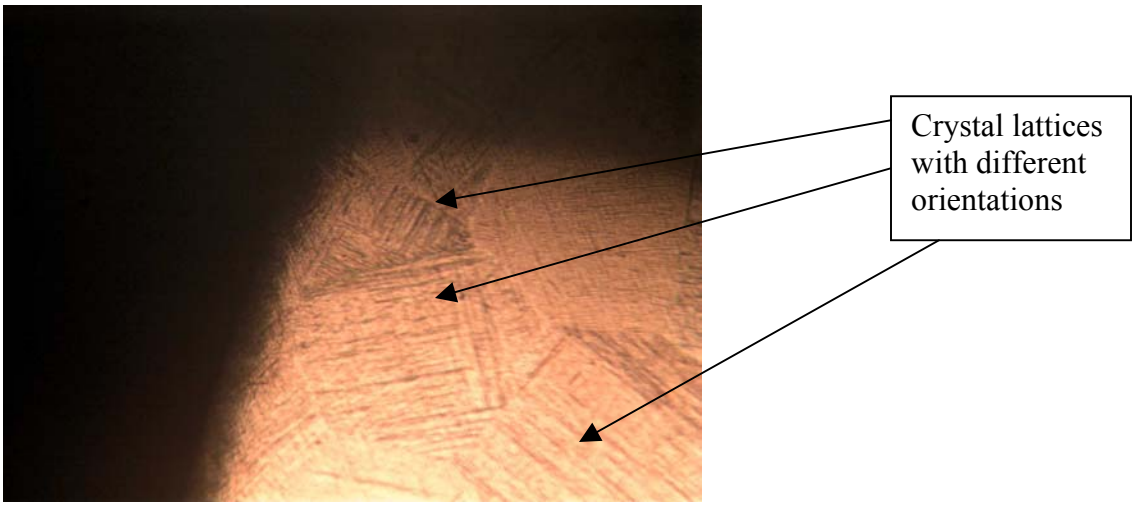

Figure 4-24 Microstructure of high speed machined specimen# 7 at 120x magnification showing the orientation of the grains.

Figure 4-25 Microstructure of conventional speed machined specimen# 6 at 120x magnification showing the orientation of the grains

4.2.4 Shape of surface defects

Figures 4-25, 4-26, 4-27 and 4-28 were taken to study the shape of the surface defects more closely. These pictures were taken at right angle to the machined surface It can be seen that the defects appear to be semispherical in shape. Figure 4-27 was taken at 200x while Figures 4-28, and 4-29 and 4-30 were taken at 250x.

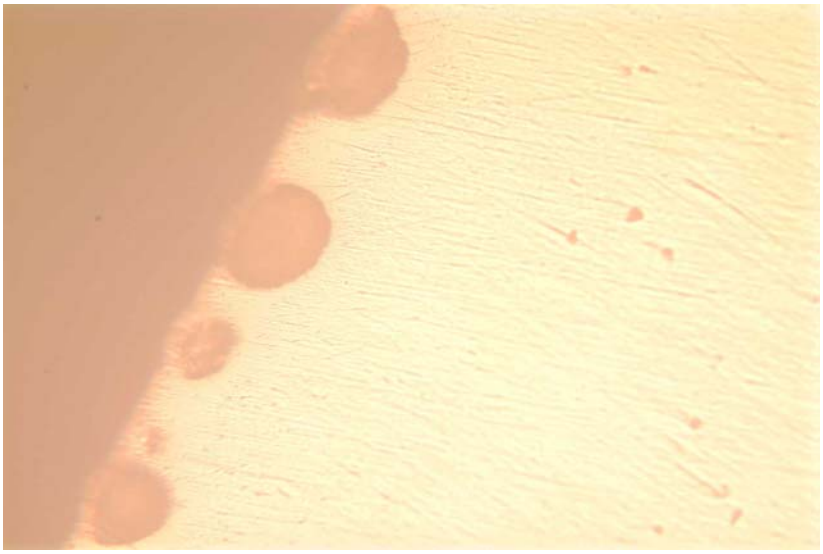

Figure 4-26 Microstructure of high speed machined unetched specimen# 6 at 200x showing the surface defects.

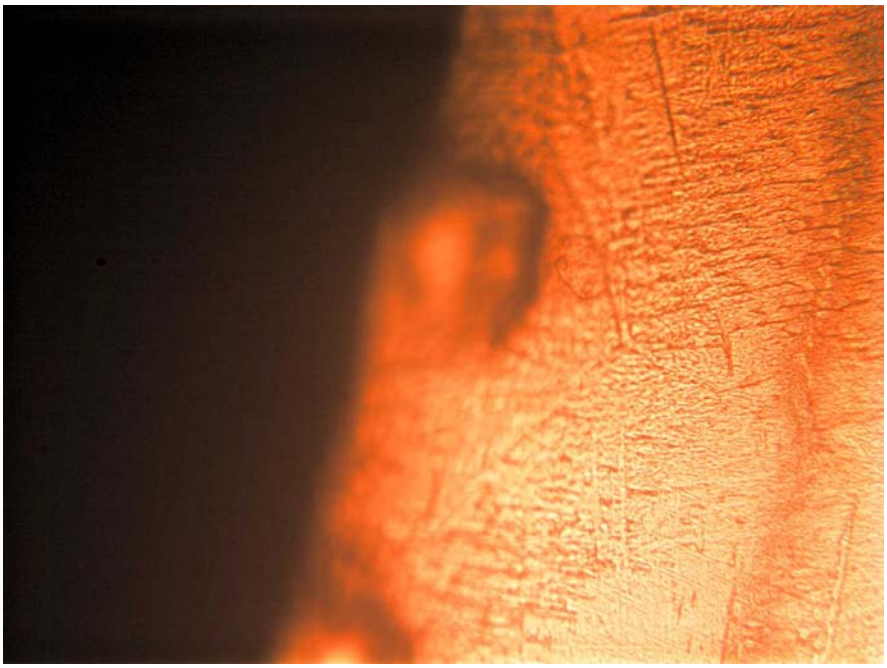

Figure 4-27 Microstructure of high speed machined etched specimen# 6 at 250x showing the surface defects at location #1

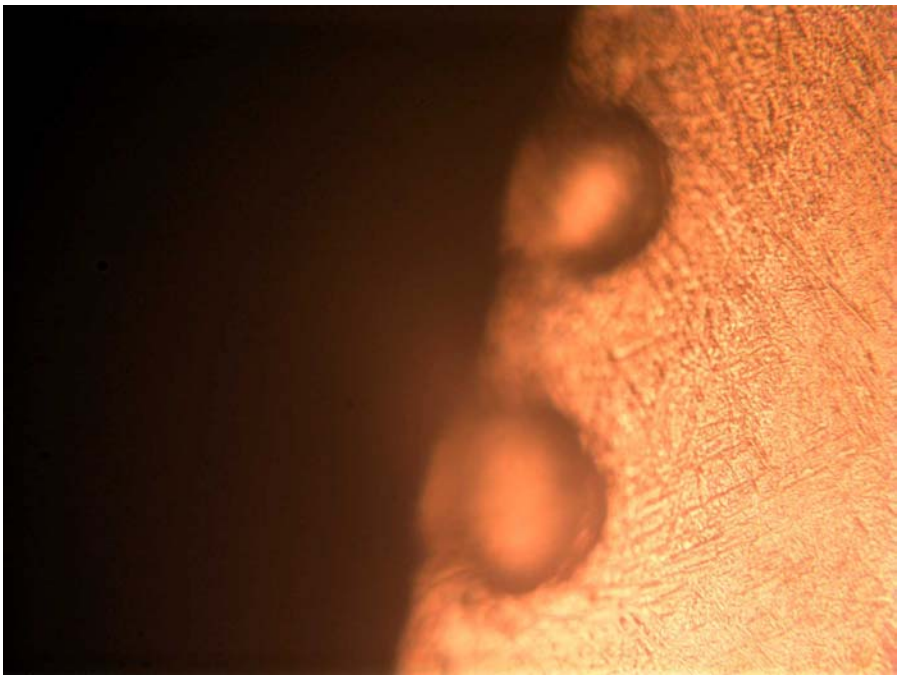

Figure 4-28 Microstructure of high speed machined etched specimen# 6 at 250x at location #2 showing the surface defects

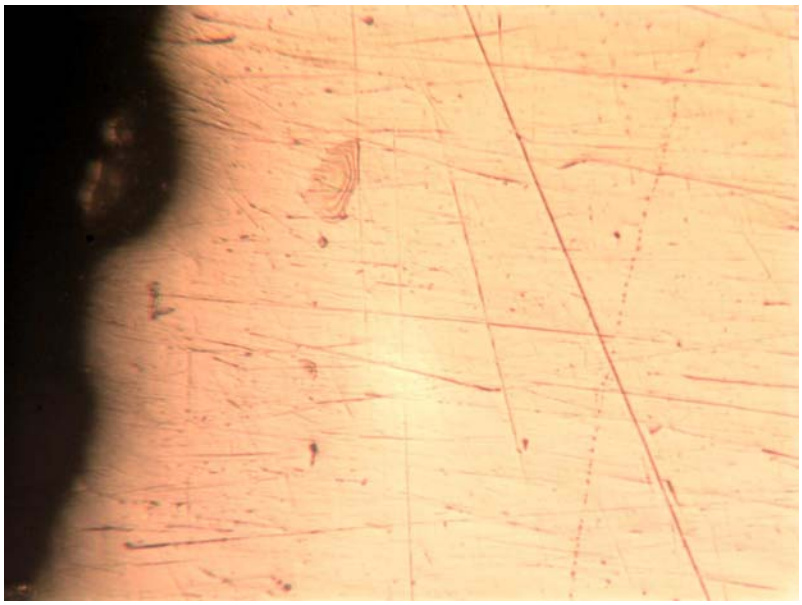

Figure 4-29 Microstructure of conventional speed machined unetched specimen# 1 at 250x showing the surface defects

The reason to take all these pictures was to note possible changes that high speed milling process has caused on the surface of Ti6Al4V as phase changes can take place in Ti6Al4V due to their direct relationship with temperature and these changes have been predicted to affect significantly the performance of components in service. Also while the temperature is what controls these transformations, cooling rate and alloy or chemical composition can all influence the temperature at which the changes take place. The metallurgy of Ti6Al4V is dominated by the crystallographic transformation, which takes place in the pure metal at 1040°C. Below this temperature, pure titanium has a hexagonal close packed structure known as alpha (α); above it, the structure is body centered cubic and termed as beta (β) [16].

The grain structure has not been changed as the grains have not grown any finer or coarser. The reason might be that the temperature produced during the high speed machining and conventional machining processes was not enough to cause any change

the grain structure of the Ti6Al4V specimens. The maximum temperature produced in the workpiece during the conventional and high speed machining processes occurs at the shear plane, which was calculated by using the program written in Matlab (software) which is presented as follows:

```
% Calculation of shear plane temperature for the high speed machining of Ti6Al4V [3].

% v = cutting speed in m/sec

% al= rake angle in radians

% aldeg= rake angle in degrees

% con  = workpiece thermal cond.

% cont = tool thermal cond

% phi = shear angle

% rhoc = sp heat per unit vol of wkpc

% Ts = shear plane temp

% r = chip ratio

% b = axial depth of cut


for n=1:100

   r(n)=0.01*n;

aldeg=-5;

v=1.06;        % velocity is in m/sec

Ks=2000; %Specific force in N/mm^2

h1=0.2032
```

```
h2(n)=h1/r(n); % h1 and h2 are in mm
con=7.2; %con=7.2 for Ti6Al4V alloy
cont=70;
rhoc=2.7; %rhoc=2.7 J/kg K for Ti6Al4V
b=3.175; % b is in mm
al=aldeg*pi/180;
phi(n)=atan((r(n)*cos(al))/(1-r(n)*sin(al)));
beta=17*pi/180;
Ts(n)=Ks*cos(phi(n)+beta)/(rhoc*cos(phi(n))*cos(beta))+20
end
plot(r,Ts)
xlabel('chip ratio')
ylabel('Shear Plane Temperature (deg C)')
title('Variation of Shear plane temperature with chip ratio for machining Ti6Al4V')
gtext('High speed machining')
gtext('chipload = 0.2032 mm (0.008")')
gtext('cutting speed = 1.06 m/sec (63.64 m/min)')
gtext('axial depth of cut = 3.175 mm (1/8")')
```

Figure 4-30 shows that for different values of chip ratio the shear plane temperature never exceeded the transformation temperature of Ti6Al4V which is 1040°C, so it can be said there is no impact of high speed machining and conventional machining processes on the grain structure of the material. The grain structure refers to grain orientation, shape and size. By refining the microstructural unit size, e.g., grain size

material's resistance to crack nucleation and microcrack growth can be improved [17]. A brief theory of grain refinement by phase transformation is discussed in 4.3.

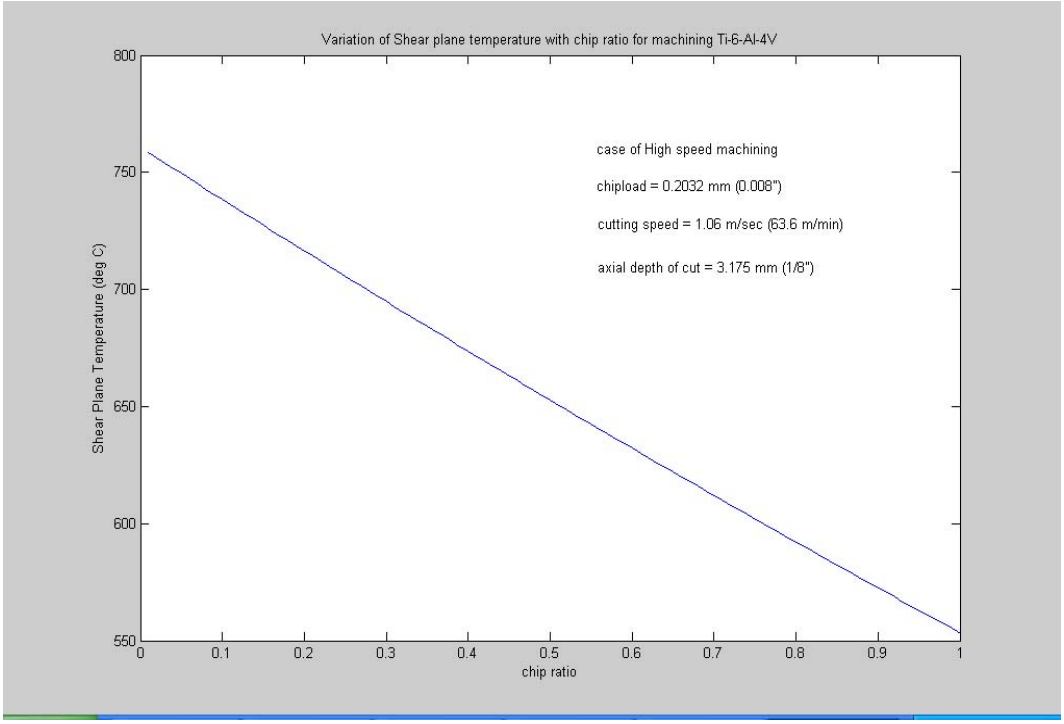

Figure 4-30 Variation of shear plane temperature with chip ratio

4.3 Grain Refinement by Phase Transformation

Several studies have shown that repeated thermal cycling of a material through a phase transformation can result in a very fine grain size. The mechanism of grain refinement is the nucleation of the reaction product at several sites on the grain boundaries of the parent phase. The product phase then grows as the transformation proceeds, replacing the single parent grains by a multitude of smaller grains. Repeated cycling through the phase transformation further refines the structure until a saturation grain size is reached [17].

4.4 Rockwell C Hardness Test

The Rockwell C Hardness test is a hardness measurement based on the net increase in depth of impression as a load is applied. Hardness numbers have no units. The test was carried out on all the machined specimens to note the changes in the hardness of Ti6Al4V specimens which were machined using different machining parameters.

Table 4-2 Rockwell C hardness test measurements for specimen #2, #7 and #8

	ROCKWELL C HARDNESS TEST MEASUREMENTS					
	Conventional Speed Machined		High Speed Machined		Special set of parameters	
Sr. No.	SPECIMEN # 2		SPECIMEN # 7		SPECIMEN # 8	
1	36.1		37.5		35.6	
2	35.8		37.0		35.6	
3	35.5		37.0		35.8	
4	36.4		37.9		36.0	
5	36.6		37.4		36.3	
6	36.8		37.5		34.4	
Average	36.22		37.36		35.62	

Tables 4-2 and 4-3 show the hardness test results that were obtained on specimens machined with different set of machining parameters. By comparing the average hardness values of high speed machined and conventional speed machined specimens in Tables 4-2 and 4-3, it can be noticed that there is a slight increase in the hardness of the high speed machined specimens as compared to the conventional speed machined specimens.

Table 4-3 shows the data of the hardness testing performed on specimen #1,#6 and #5.

Table 4-3 Rockwell C hardness test measurements for specimens #1, #6 and #5

	ROCKWELL C HARDNESS TEST MEASUREMENTS					
	Conventional Speed Machined		High Speed Machined		Special set of parameters	
Sr. No.	SPECIMEN # 1		SPECIMEN # 6		SPECIMEN # 5	
1	36.1		36.3		35.0	
2	36.1		36.6		36.5	
3	36.2		36.1		36.2	
4	36.7		37.4		36.1	
5	35.2		37.1		36.3	
6	36.4		36.7		36.3	
Average	36.12		36.78		36.28	

An analysis of variance was performed by Sharath Cugati on the Rockwell C hardness test data and the results included in Table 4-4 indicate that hardness is affected

by the machining processes and this effect is independent of the specimens. There may be an interaction but this might be an artifact of the strong process dependence.

Table 4-4 Analysis of Rockwell C hardness data

	SUM OF SQUARES	DEGREES OF FREEDOM	MEAN SQUARE	F STATISTIC	PROBABILITY
PROCESS	9.282222	2	4.641111	17.76313	8.14×10^{-6}
SPECIMEN	0.100278	1	0.100278	0.383798	0.540255
INTERACTION	1.928889	2	0.964444	3.691261	0.03688
WITHIN	7.838333	30	0.261278		
TOTAL	19.14972	35			

Table 4-5 Rockwell C hardness data grouped by process

PROCESS	MEAN	STANDARD DEVIATION
CONVENTIONAL	36.15833	0.477604
HSM	37.04167	0.536755
SPECIAL	35.841667	0.617117

Since Table 4-4 indicates the probability that the hardness will not be affected by the machining process is 0.000814, it means that the hardness would definitely be affected by the process adopted to machine the workpieces. Also the probability that the variation in the hardness between the specimens taken out from the same machined area would merely be affected by a chance is 54.02% which implies that the specimens from the same machined area would not differ much in the hardness

From the Table 4-5, it can be observed that differences in the mean values of hardness of the specimens, machined using three different sets of parameters, is small.

After machining the workpiece using advance speed machining parameters a finish machining pass was made and microstructural study of the specimen was carried out. Figures 4-31, 4-32, 4-33, and 4-44 shows the micrographs of the specimen taken at four different locations at right angle to the machined surface. The scale used for all the micrographs is a 1 mm scale and each division is of 10 microns.

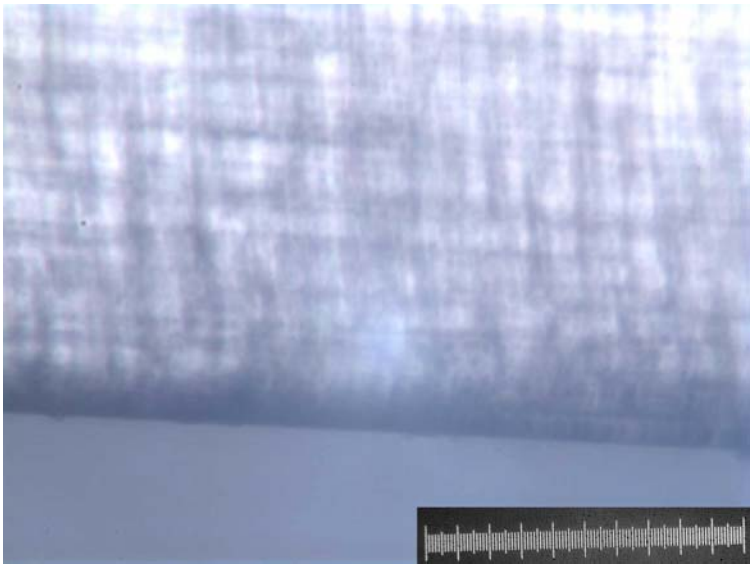

Figure 4-31 Microstructure of the advance speed machined specimen after the finish machining pass at location #1 at 100x magnification

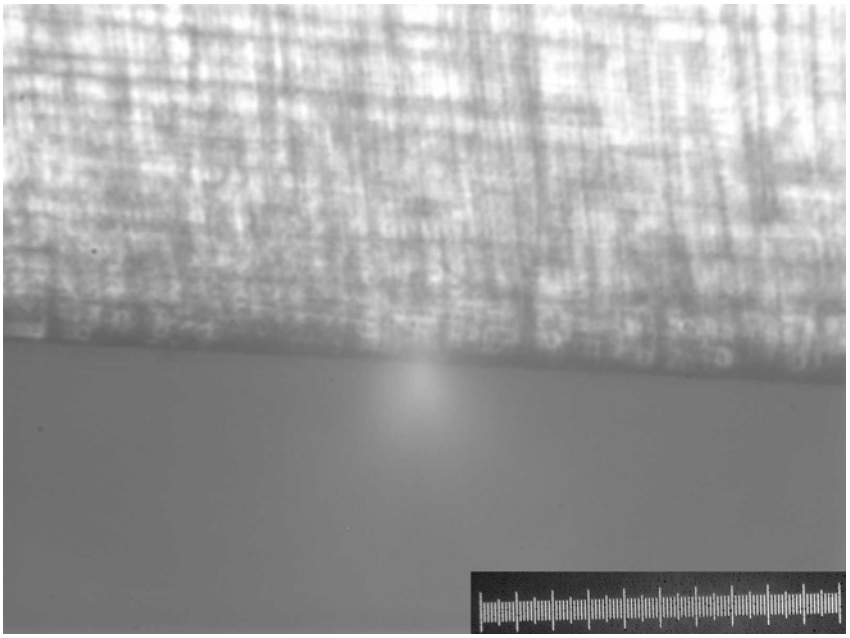

Figure 4-32 Microstructure of the advance speed machined specimen after the finish machining pass at location #2 at 100x magnification

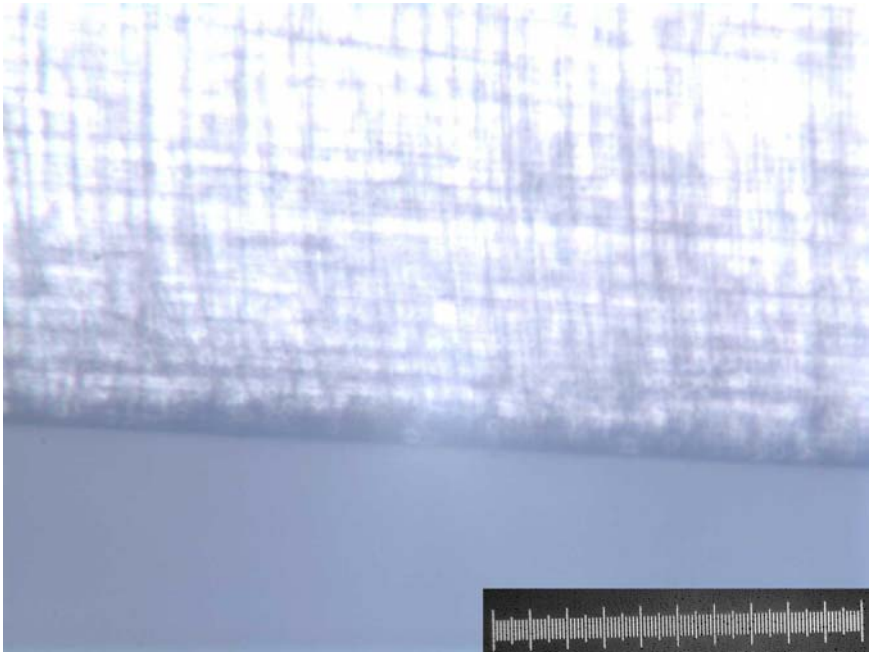

Figure 4-33 Microstructure of the advance speed machined specimen after the finish machining pass at location #3 at 100x magnification.

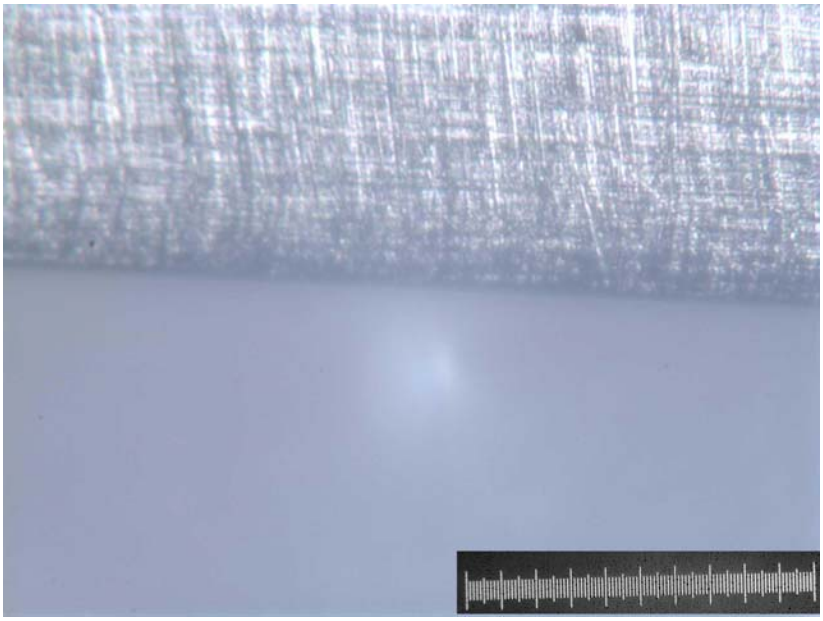

Figure 4-34 Microstructure of the advance speed machined specimen after the finish machining pass at location #4 at 100x magnification

By observing Figures 4-31, 4-32, 4-33 and 4-44, it can be seen that no surface defects were visible at right to the machined surface as the finish machining pass was able to remove the surface defects that were formed due to the advance speed machining process. So a finish machining pass proved to be a good solution for maintaining the surface integrity of the workpiece.

CHAPTER 5
DESCRIPTION OF INSTRUMENTS AND METHODS

This chapter presents the specifications of the machine tool structure, fixture, workpiece, cutters and different instruments used to carry out the machining tests of Chapter 3 on the specimens Also, this chapter elaborates the procedure for carrying out these tests.

5.1 Description of Machine Tool used

The machine tool used for machining was HVM 600 A from Ingersoll. The HVM (High velocity module) uses a box type frame to provide rigid support on both the top and bottom of the moving axis. The X-axis gantry rides on ways and is driven both on top and bottom by linear motors. As a result there are no cantilevered and overhung loads and the structure has high stiffness-to-weight ratio compared to conventional machines. The Y- axis saddle rides up and down on the gantry and is similarly driven on each side by a pair of linear motors, thus also being symmetrical about the spindle as well as the X axis gantry. The Z-axis horizontal ram is center mounted in the saddle and is driven by a linear motor arranged below the ram [19].

5.1.1 Specifications of Machine Tool structure

The speed range for its spindle is 0 – 20000 rpm. The tool adaptation is HSK63A. Maximum continuous power is 37.5KW and maximum continuous torque is 45Nm. One of the reasons to choose this machine for doing cutting tests was that it has a flood coolant capability, which allows the tool chip interface to always remain in the cover of coolant during machining [19].

5.1.2 Tool storage option

The tool storage has 40 pockets and is a direct load chain type. The maximum tool weight is 25 lbs [19].

5.1.3 Axes designation and their travels

The X axis denotes the longitudinal travel of the gantry and is perpendicular to Y-axis. The axis travel for X axis is 24.803''. The Y axis specifies the vertical travel of the saddle and travel for Y axis is 24.803''. The Z axis denotes the horizontal travel of the ram and is perpendicular to Y axis. The travel for Z axis is 23.622''.B axis denotes the rotational travel of the index table and has a rotational travel of +/-360degrees. A-axis denotes the axis pallet exchanger. This rotary axis moves the pallet from the workload station into the work area of the machine and has the rotation of +/-180 degree [19].

5.1.4 Feedrates

The feedrates for the 3 axes are as follows [19]:
X axis = 3000 IPM.
Y axis = 3000 IPM.
Z axis = 3000 IPM.

5.1.5 Lubrication system

The lubrication system of Ingersoll lubricates the X, Y and Z axes slides and the tool changer. It consists of a Trabon lubrication system, a reservoir containing Mobilux EP 1 grease, and the lubrication circuitry. The lubrication system is controlled and monitored by the PMC logic. The PMC cycle initiates the lube cycle until all ways and tool changer have received their designated amount of lubrication. If the lubrication cycle fails, logic delays and sends the end of block (EOB) stop request to the CNC and displays a message on the alarm screen [19]

5.2 Fixture

Initially the cutting tests were carried out using vise as the fixture but the work part chattered which posed limitations on the depth of cut. The specimens were then mounted on the tombstone. The tombstone is a square block made of cast iron with slots for holding the specimens using clamps. The reason for selecting the tombstone was to provide higher stiffness to the work part in order to avoid chatter.

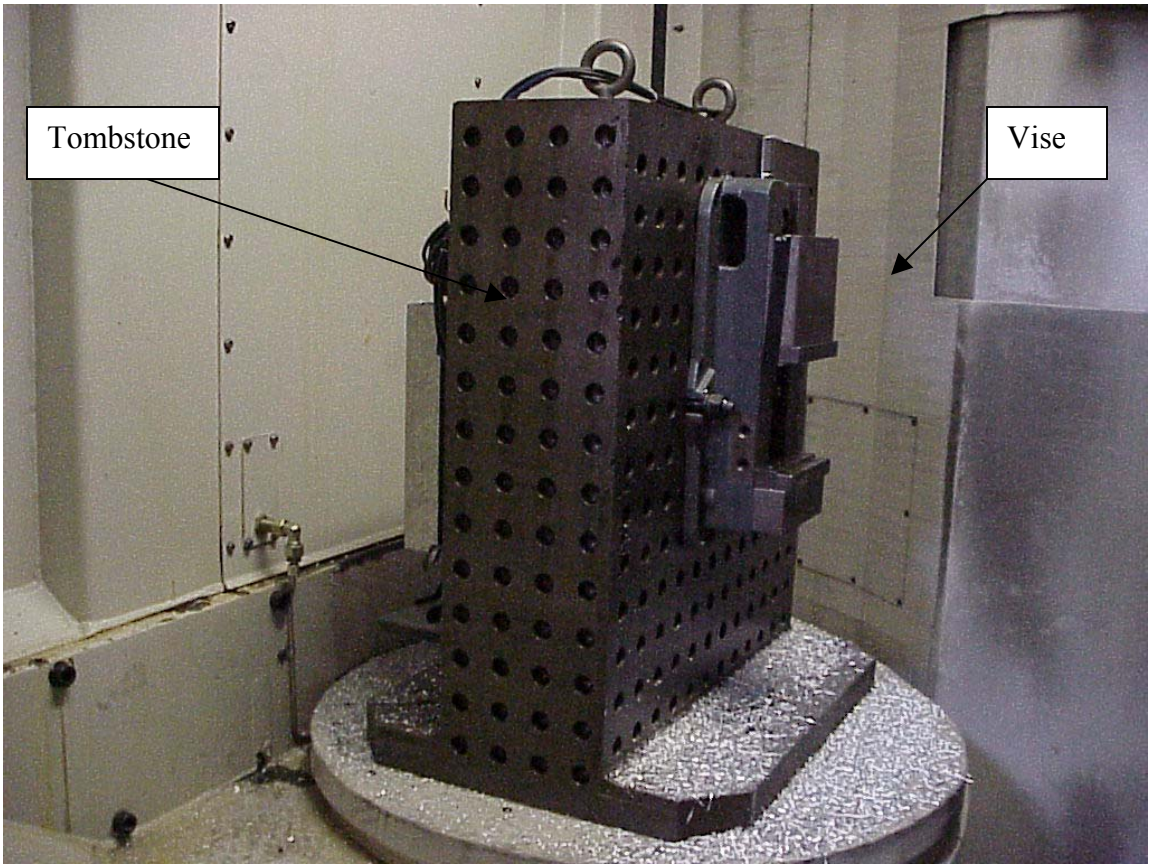

Figure 5-1 A vise clamped to Tombstone

5.3 Workpiece

Specimens made of Ti6Al4V alloy were used as the workpiece for carrying out the cutting tests .Each of these specimens has dimensions of (19.5inch x 3.5inch x 1 inch).

Figure 5-2 Workpiece used for cutting tests.

5.4 Cutter and inserts

A 3-inch diameter face mill with 4 coated carbide inserts was used to machine the Ti6Al4V parts. The ISO designation for the insert used is LFHW 220480FNLN [20].

5.5 Type of coolant used

The type of coolant used was Quantalube 275 (Cincinnati Milacron, Cincinnati, Ohio).

5.6 Hardness Tester

The Rockwell hardness tester has the capability of testing metals having a wide range of hardness. This capability is obtained by using different combinations of load and penetrator. The two most common combinations are 100 kg major load applied to a 1/16 diameter ball to give a B hardness number and a 150 kg major load applied using a diamond (brale) shaped penetrator to give a C hardness number [13]. Figure 5.3 shows the picture of the hardness tester used for doing the Rockwell C hardness test on the machined specimens.

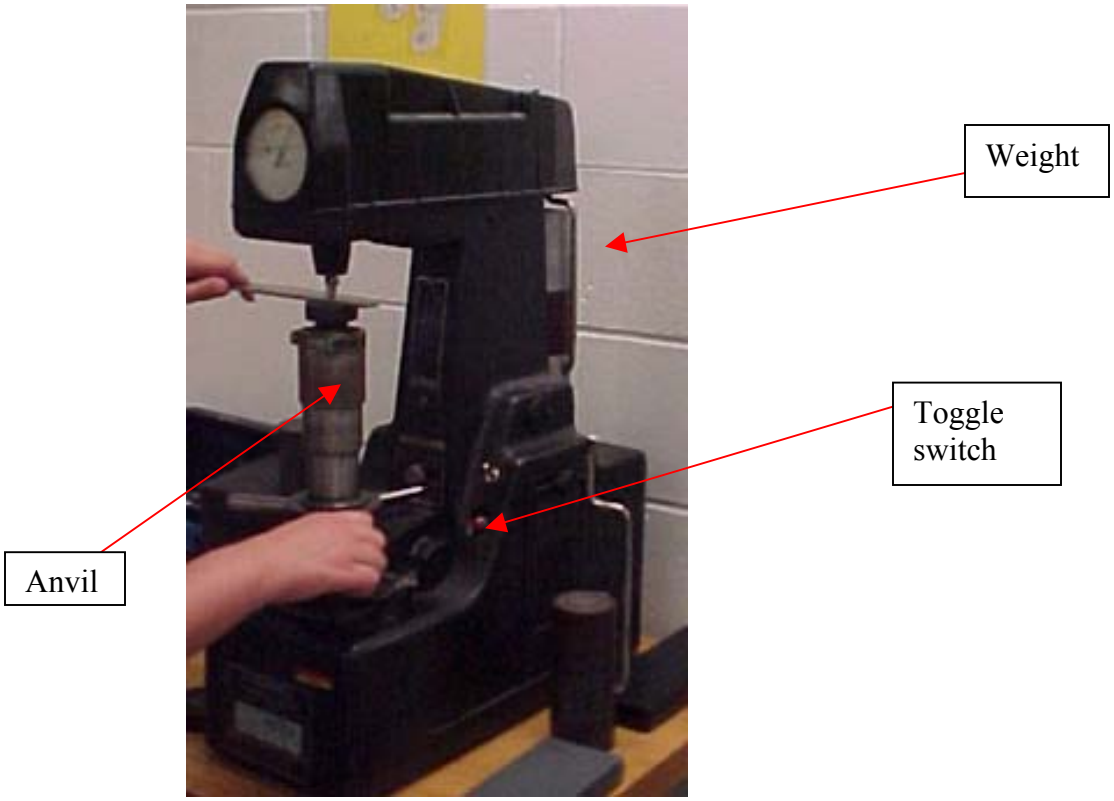

Figure 5-3 Hardness tester

Procedure for performing the hardness test on hardness tester

1. The machine is turned on by using a toggle switch.
2. The correct weight of 150 kg is installed at the back of the tester.
3. Diamond tip is then inserted and is tightened using the setscrew.
4. The specimen is then placed on the anvil.
5. The wheel is then turned clockwise until the specimen touches the tip. The wheel is continued to turn until the small dial on the face of the machine is pointing towards the dot. The dialed is then turned to zero using the thumbwheel.
6. The lever below the thumbwheel is then pressed to start the process of taking measurement.
7. The test is automatically performed and the hardness number is read from the black scale.

5.7 Optical Microscope

An optical microscope shown in Figure 5-4, available in the Material Science Department at the University of Florida, was used to carry out the metallographic study of the Ti6Al4V specimens

Figure 5-4 Optical Microscope

The components of the optical microscope shown in Figure 5-4 are:

1. Standard Damped Worktable
2. Console Unit
3. Incident Light
4. 100W Halogen and 150W Xenon Light Source
5. Large centerable Rotation Stage
6. 4X4 Stage Coaxial XY control
7. Binocular Tube
8. Camera Cone & 545 Polaroid Film back
9. Color Camera & Monitor

In conclusion each instrument that is described in this chapter had played an important role in finding the possible effects of high speed machining and conventional speed machining processes on the Ti6Al4V surfaces The specifications of the Ingersoll, (55 HP, 45 N-m peak torque) [19], provided the necessary power and torque required for the cutting tests. The tombstone, as the workholding fixture, provided the necessary stability to the workpiece during machining. The camera attached to the optical microscope, interfaced with the computer, provided a useful capability of interacting with the surface topography of Ti6Al4V at different levels of magnifications.

CHAPTER 6
CONCLUSIONS AND RECOMMENDATIONS

The Ti6Al4V workpieces were machined using conventional machined and high speed machined parameters calculated at MTRC and the results of metallographic study indicate that high speed milling process produces more surface defects than the conventional machining process. The results have shown that these surface defects do not have any specific sites of occurrence on the grain boundaries but instead they can occur on any part of the grains. These surface defects are stress concentration areas and may act as sites for the earlier initiation of fatigue cracks leading to lower fatigue life.

Microstructure analysis has also shown that there is no change in the size of the grains of a high speed machined sample and a conventional speed machined sample as the grains did not grow any finer or coarser. Also the results have shown that there is no specific orientation of all the grains as a result of high speed machining rather there is an abrupt change in the crystal orientation as was expected in a general polycrystalline material. So, the effects of high speed milling on the grain size and orientation can be neglected These otherwise would have caused a difference in the mechanical properties of the material according to the Hall-Petch relationship which states that yield strength is approximately inversely proportional to the square root of the grain diameter [3].

Rockwell C hardness testing shows that the high speed machined specimens average slightly higher hardness than the conventional speed machined specimens. The results indicate that the hardness is affected by the machining processes. From all the above results it is clear that the top layer of the surface is damaged more severely due to

high speed milling process than with the conventional milling process but this damaged layer is only a few microns thick. So a finish machining pass was made over the high speed machined area to remove the damaged layer that resulted in the removal of the semispherical defects which helped in maintaining the surface integrity of the workpiece.

6.1 Recommendations

In conclusion, while titanium alloys present a unique set of machining problems, many of those problems can be alleviated or eliminated by adhering to the following set of guidelines:

1. Performing shallow finish machining pass to remove the damaged layer.
2. Using large volumes of recommended cutting fluids.
3. Using abrasion and heat resistant cutting tools.
4. Replacing cutting tools at the first sign of wear.

6.2 Future Work

Various machining tests can be performed to see what is in the machining process that leads to the formation of the semispherical defects on the surfaces of Ti6Al4V.. After the fatigue testing on these specimens a comparison for the fatigue lives can be made to check for changes in the fatigue life. Fatigue crack initiation and growth can be modeled by determining the fatigue crack initiation sites and then causes for the failure of the specimens from these sites can be correlated with the changes in the machining parameters.

LIST OF REFERENCES

1. "The Online Material Information Resource," Internet Literature http://www.hanita.com/hanita_protected/hanita-art3.htm, 06/02/03.

2. Rodney B, Gerhard Welsch, Collings E W "Materials Properties Handbook," ASM International, Materials Park, OH, 1994.

3. Tlusty, J. "Manufacturing Processes and Equipment," Prentice Hall, Upper Saddle River, NJ, 2000.

4. Cugati, S. A., "High Speed Machining Of a Helicopter Magnesium Gearcase," Master's Thesis, University of Florida, August 2002.

5. Yousuf Ahmed, "High Speed Machining Of An Alumnium Aircraft Gearcase," Master's Thesis, University of Florida, 2000.

6. Martin, C. L., "Optimization of Machining Operations for an Aerospace Component made from Titanium Alloy Ti-6Al-4V," Master's Thesis, University of Florida, May 2000.

7. Titanium: A Technical Guide, ASM International, Materials Park, OH, 44073-0002, page 75-85, 1988.

8. Schutz R. W. and Thomas D. E. "Corrosion of Titanium and Titanium Alloys," Metals Handbook-Ninth Edition, Vol. 13-Corrosion, ASM, Materials Park, OH, 1987

9. "The Online Material Information Resource," Internet Literature www.steelforge.com/infoservices/matoverview/mo_titanium.asp, 07/04/03.

10. "The Online Material Information Resource," Internet Literature http://www.engr.sjsu.edu/WofMatE/projects/srproject/srproj5.html, 08/05/03.

11. "The Online Material Information Resource," Internet Literature http://www.azom.com/details.asp?ArticleID=1547, 08/08/03.

12. "The Online Material Information Resource," Internet Literaturewww.unl.edu/nmrc/Diesinking/surfaceint/surface.html, 08/22/03.

13. Kakiel A. M. "Process Improvements in Milling Titanium Alloy Ti-6Al-4V," Master's Thesis University of Florida, August 1999.

14. S. Suresh “Fatigue Of Materials,” Cambridge University Press, 110 Midland Avenue, Port Chester, NY 10573, 1991.

15. “The Online Material Information Resource” Internet Literature www.njpt.com, New Jersey Precision Technologies, Inc., 08/30/03.

16. VanderVoort. G. F “Principles Of Metallography,” McGraw-Hill Book Co. 1221 Avenue of Americas, NY 10020, 1984.

17. Berg J. Kiese, Wagner L, **“**Crack Propagation In Gradient Microstructures in Titanium Alloys,” Technical University of Brandenburg at Cottbus, 03013 Cottbus, Germany, 1997.

18. Walter J.L., Westbrook J.H., Woodford D.A. “Grain Boundaries In Engineering Materials,” Baton Rouge LA. 70821, 1974.

19. High Velocity Module, The Ingersoll Milling Machine Co., Rockford, Illinois, 1996.

20. Kennametal Inc., Kennametal Milling Catalogue 8040, Metalworking Systems Division, Latrobe, PA 15650, 1998.

BIOGRAPHICAL SKETCH

The author was born on August 6, 1979, in Chandigarh, India, where he grew up and had his initial schooling. He attended the G.Z.S.C.E.T College of Engineering and Technology in Punjab, which was affiliated with the Punjab Technical University. He earned the Bachelor of Science degree in mechanical engineering in 2001. During his undergraduate degree he completed his internship from Punjab Tractors Limited (PTL) which is India's second largest manufacturer of tractors. While working at PTL he developed his interest to go for higher studies and he moved to Gainesville, Florida, to pursue his Master of Science degree in mechanical engineering at the University of Florida.